

1

# NOvA Test Beam detector calibration

2

## Technical Note

3

Robert Kralik

University of Sussex

4

September 22, 2023

5

### Abstract

6

What is this about and what will I describe in here

7

## Contents

8	<b>1</b>	<b>Introduction</b>	<b>2</b>
9	<b>2</b>	<b>Overview of the Test Beam detector</b>	<b>4</b>
10	<b>3</b>	<b>NOvA calibration process</b>	<b>8</b>
11	3.1	Relative calibration . . . . .	12
12	3.2	Absolute calibration . . . . .	13
13	3.3	Calibration uncertainties . . . . .	14
14	<b>4</b>	<b>NOvA Test Beam detector calibration</b>	<b>14</b>
15	4.1	Overview . . . . .	14
16	4.1.1	Definitions . . . . .	14
17	4.2	Fiber Brightness . . . . .	15
18	4.3	Simulation . . . . .	15
19	4.4	Threshold and shielding corrections . . . . .	17
20	4.5	Period 1 . . . . .	18
21	4.6	Period 2 . . . . .	18
22	4.7	Period 3 . . . . .	22
23	4.8	Period 4 . . . . .	25
24	4.9	Absolute calibration results . . . . .	29
25	4.10	Drift in TB data . . . . .	30
26	4.11	Results . . . . .	30
27	4.12	Validation . . . . .	30

# <sup>28</sup> 1 Introduction

<sup>29</sup> TO DO:

- <sup>30</sup> • Divide the motivation to abstract (why do we care about test beam calibration, what did  
<sup>31</sup> we do and how did we do it. What are the results)
- <sup>32</sup> • and introduction (brief history of test beam calibration, maybe a bit more detail into why  
<sup>33</sup> is test beam calibration important)

<sup>34</sup> History of TB calibration. What led to the final version of TB calibration. What can be  
<sup>35</sup> done next. I think this could also be in the introduction?

<sup>36</sup> Why is Test Beam? "The idea, as with any test beam experiment, is to expose a detector  
<sup>37</sup> to a beam of very well-characterized particles, so that we can improve our understanding of  
<sup>38</sup> how the detector responds to such particles. We make use of upstream detectors to collect  
<sup>39</sup> data on the beam particles before they interact in the NOvA detector. For example, we will  
<sup>40</sup> be able to see what a 1 GeV proton actually looks like in our detector, without having to  
<sup>41</sup> simulate it, and we can test how well we would have reconstructed the energy using our existing  
<sup>42</sup> techniques. We may find we are able to make improvements to our tools to better match what  
<sup>43</sup> we see in the detector with how we reconstruct it. Or we may find we already do a pretty  
<sup>44</sup> good job. Either way, with a full cross-comparison like this, we can be more confident in our  
<sup>45</sup> analysis of the data and reduce the level of uncertainty we consider are associated with the  
<sup>46</sup> relevant measured quantities. Ultimately, the aim will be to reduce the level of uncertainty on  
<sup>47</sup> the neutrino oscillation analyses and to make even better, more accurate measurements of the  
<sup>48</sup> Standard Model."Why is Test Beam calibration done:

- <sup>49</sup> • To be able to directly compare TB to the standard detectors
- <sup>50</sup> • To be able to verify our calibration procedures using TB data
- <sup>51</sup> • To study the particle response as a function of energy
- <sup>52</sup> • To determine an energy resolution
- <sup>53</sup> • To compare currently used energy scales to data and understand if we can use TB data  
<sup>54</sup> for absolute energy scale in all NOvA detectors

<sup>55</sup> For DeltaM2: By increasing exposure, total syst. error decreases by (+) 18.5%  
<sup>56</sup> Difference by reducing calib syst.: (+) 10.8% Statement: "The NOvA Test Beam will improve  
<sup>57</sup> the total systematic error on the final measurement of the oscillation parameters Dm232 and  
<sup>58</sup> sin2Th23 by 10% Potential Test Beam impacts: Check modeling of hadronic interactions in de-  
<sup>59</sup> tector (check GEANT systematics), Using Test Beam data as "single-particle MC" to train  
<sup>60</sup> CVN prong-like algorithms, Generate Adversarial Networks for MC improvements using  
<sup>61</sup> Test Beam data, Check ND calibration procedure to try and understand causes of 3-5

- <sup>62</sup> • Hadronic response and comparison with MC modeling
  - <sup>63</sup> – response as a function of energy
  - <sup>64</sup> – establishing of an absolute energy scale

- 65        – determination of energy resolution
- 66        – studies of topological features and resolution
  - 67            \* pion tracking and showers
  - 68            \* proton tracking and showers
- 69        – studies of timing features and resolution
- 70     • Electromagnetic response and comparison with MC modeling
  - 71            – response as a function of energy
  - 72            – establishing of an absolute energy scale
  - 73            – determination of energy resolution
  - 74            – studies of topological features and resolution
    - 75              \* electron signatures
    - 76              \* gamma signatures
  - 77            – studies of timing features and resolution
  - 78            – studies of  $\pi^0$  from  $\pi^-$  charge-exchange
- 79     • Muon response and comparison with MC modeling
  - 80            – comparison with detailed optical simulations
  - 81            – determination of energy resolution
  - 82            – studies of topological features and resolution
  - 83            – cross-talk studies
  - 84            – comparison to cosmic ray muons (requires a special trigger)
  - 85            – studies of the muon calibration protocol
- 86     • Light yield and response studies as a function of particle type and detector configuration
  - 87            – understanding the Cherenkov light contribution
  - 88            – vertical and horizontal responses and comparison with simulations
  - 89            – data with selected planes rotated by 45 and 90 degrees
  - 90            – slanted (angle) plane response (and subset of programs as above)
  - 91            – fiber attenuation studies
  - 92            – Birks' constant studies
- 93     • Near / Far readout comparison
- 94     • Gather large libraries of particles at known energies and multiple angles of incidence to
  - 95            help develop a CNN prong ID. Also allows training of a particle-based CVN-like PID.

96     Also use information from:

- 97        • NOvA Test Beam Technical Statement of Work

- 98     • NOvA Test Beam program (paper for DOE) [docdb:25074]  
 99     • NOvA Test Beam task force report [docdb:15750]  
 100    • Overview presentation of NOvA Test Beam [docdb:20495]  
 101    • Test Beam support document [docdb:22172]  
 102    • NOvA Test Beam program proceedings [docdb:55808]  
 103    Mike's proceedings from ICHEP 2020 [1].

## 104    2 Overview of the Test Beam detector

105   The NOvA Test Beam detector is a scaled down version of the near and far detectors shown on  
 106   figure 1. It is placed in the MC7b enclosure of the Fermilab Test Beam Facility in the path of  
 107   the MCcenter beamline with a variety of beamline detectors to measure and identify a range of  
 108   particles with various momenta [2].

109   Majority of the Test Beam detector and it's instrumentation is identical to the other NOvA  
 110   detectors, with a few exceptions that could have an impact on the calibration. We are going to  
 111   identify and discuss these differences in this section.

112   Should I aslo talk about the beam halo? Could that have an influence on the calibration?  
 113   Maybe it's the peaks in the cosz distribution?

114   Mention the exact times that Test Beam operated in including the individual data taking  
 115   period Dates and times when the data taking occured.

116   The Test Beam detector started with commissioning runs in May 2019 and it was finally  
 117   shut down on midnight of July 9<sup>th</sup>, after which it was decommissioned. The full data taking is  
 118   split into periods divided by the regular Fermilab summer shutdown of the beam. The Test  
 Beam data periods are:

Period 1	March 22 <sup>nd</sup> 2019	-	July 6 <sup>th</sup> 2019
Period 2	December 5 <sup>th</sup> 2019	-	March 20 <sup>th</sup> 2020
Period 3	January 12 <sup>th</sup> 2021	-	June 27 <sup>th</sup> 2021
Period 4	November 30 <sup>th</sup> 2021	-	July 10 <sup>th</sup> 2022

Table 1: Test Beam detector data taking periods.

119

### 120   General parameters

121   The NOvA Test Beam detector consists of two 31-plane blocks, each beginning and ending  
 122   with a vertical plane, with an additional horizontal plane glued inbetween them to preserve the  
 123   alternating pattern [3]. Each plane consists of 2 modules side-by-side, each module made up of  
 124   32 cells. Each cell is 2.6 m long with an inner (without the PVC) depth and width of 5.9 m and  
 125   3.8 cm respectively, same as for the other NOvA detectors. This brigns the final dimensions of  
 126   the Test Beam detector to 63 planes  $\times$  64 cells, or  $2.6 \times 2.6 \times 4.1 \text{ m}^3$ .

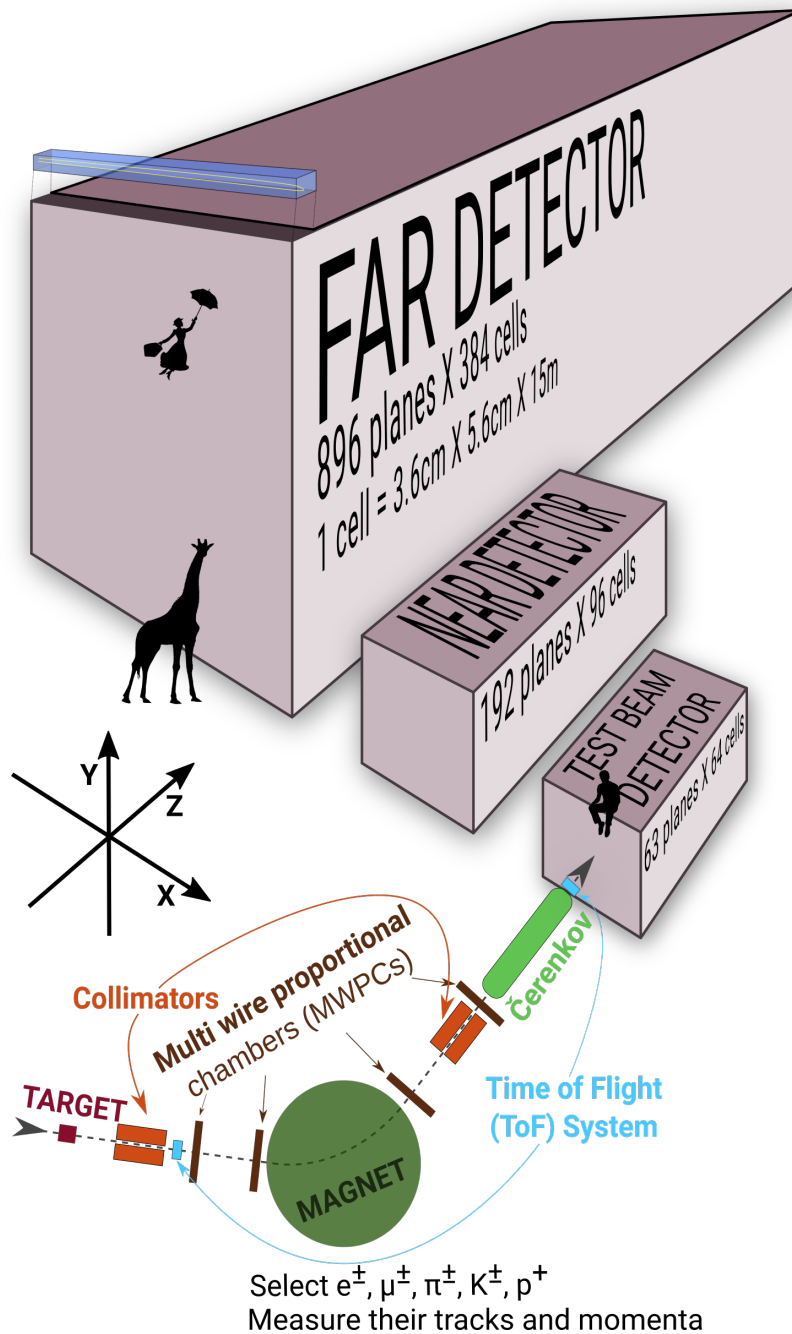


Figure 1: Comparison of Test Beam detector scale to the Near and Far NOvA detectors (and a man, giraffe, or Mary Poppins). Also shown are the Test Beam beamline detectors and components (not to scale), with arrows showing the direction of the beam. The three black arrows show the orientation fo the detector coordinate system.

<sup>127</sup> The 63 planes are numbered from 0 to 62, with even numbers corresponding to vertical  
<sup>128</sup> planes and odd numbers to horizontal planes. Cells are numbered 0 to 63, going from bottom  
<sup>129</sup> to top for horizontal planes and left to right, when facing the front of the detector, for vertical  
<sup>130</sup> planes.

<sup>131</sup> The detector coordinate system is illustrated on figure 1. It is centered with (0,0,0) in the

<sup>132</sup> centre of the first plane [4]. The x axis runs left to right when facing the front of the detector,  
<sup>133</sup> y axis bottom to top, and z axis goes along the beam direction from front to the back of the  
<sup>134</sup> detector. Position within each cell ( $w$ ) is aligned with the x (y) axis for the horizontal (vertical)  
<sup>135</sup> cells, with  $w = 0$  centered in the middle of each cell. The exact geometry of the Test Beam  
<sup>136</sup> detector was measured in several alignment surveys and is saved in gdml files [5].

<sup>137</sup> In the past we encountered an issue when trying to align the Test Beam detector with the  
<sup>138</sup> beamline measurements by rotating the detector. This broke several assumptions within the  
<sup>139</sup> Test Beam geometry [4] and manifested as uncalibrated cells in the back of the detector [6].  
<sup>140</sup> This was fixed by realigning both the detector and the beamline separately, based on the last  
<sup>141</sup> alignment survey, measured during the decommissioning of the detector. We implemented the  
<sup>142</sup> fix in the production tag R23-04-05-testbeam-production.a [4].

### <sup>143</sup> Scintillator

<sup>144</sup> The Test Beam detector is filled with several different versions of the NOvA scintillator oil,  
<sup>145</sup> which differ mainly in the way they were stored since the filling of the near and far detectors.  
<sup>146</sup> This is illustrated on figure 2.

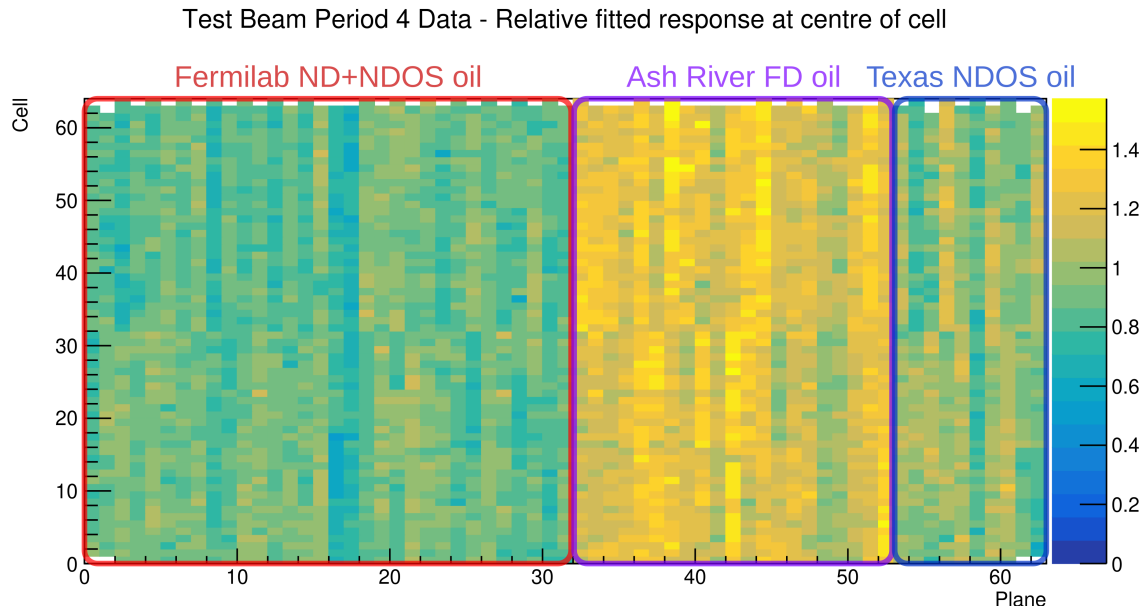


Figure 2: Uncorrected energy response in the centre of cells across the Test Beam detector showing a clear distinction between the different scintillator oils.

<sup>147</sup> The scintillator oils used in the Test Beam detector are:

- <sup>148</sup> • Oil stored in a tanker and tanks outside in Fermilab [7];
- <sup>149</sup> • ND production oil (is it ND prod or NDOS or what?) stored underground in barrels at  
<sup>150</sup> MiniBooNE [8];
- <sup>151</sup> • FD production oil stored inside at Ash River in "totes" under several layers of black  
<sup>152</sup> plastic [9];

- 153 • NDOS-drained oil stored mainly inside in Texas A&M University and University of  
154 Texas at Austin [10, 11].

155 The original plan [12] was to use the tanker and tank scintillator for the entire Test Beam  
156 detector. However, due to extreme cloudiness of the scintillaotr in the tanks

157 The original plan [12] was to use the scintillator from a tanker and one of the tanks located  
158 outside in Fermilab. First tests showed acceptable results and the tanker oil was used to fill out  
159 almost the entirety of the first block of the detector (first 32 planes) [7]. However, when we  
160 loaded the oil from tank two into the tanker, it became extremely cloudy and unusable, possibly  
161 due to contamination with water accumulated at the bottom of the tanks, which was mixed with  
162 oil by the pump. The rest of the first block was the topped up with high quality scintillator  
163 from NDOS, which has been stored inside in barelles at MiniBooNE [8]. This is labeled as  
164 "Fermilab ND+NDOS oil" on figure 2.

165 Even before the extreme cloudiness was discovered, it was known that the oil from the tanks  
166 has lost much of its original light yield properties. Reasons vary from water contamination to  
167 insects and dirt contamination [13]. Yet it was still decided to use the tank 2 oil [12]. It was  
168 also decided not to mix the various oils (tanker/tank/NDOS/Ash River) as studying energy  
169 deposition in different types of oils could lead to some interesting insights [13].

170 The first 21 planes of the second block (planes 32 to 52) were filled with the Far Detector  
171 production scintillator shipped in from Ash River [14]. This oil has been stored in "totes"  
172 inside a building and under several layers of black plastic [9]. Also used a little (70 gallons)  
173 scintillator from NDOS to fill these planes (compared to 1900 gallons from Ash River) [14].

174 The last 10 planes (planes 53 to 62) [14] were filled with scintillator drained from NDOS  
175 stored in Texas A&M University and University of Texas at Austin [10, 11]. This scintillator  
176 has higher light yield than the one from the tanker, but lower than the Ash River one [10].

177 In total the Test Beam detector is filled with 5418 gallons of scintillator oil with a weight  
178 of approximately 28.6 tons [3].

## 179 **Readout**

180 The Test Beam detector uses in total 126 front end boards (FEBs), each reading out signal from  
181 32 cells (half of a plane) [3]. The readout is located on the top and right (looking on the front)  
182 side of the detector. 118 FEBs are version 4.1, same as in the Far Detector, and 8 FEBs, located  
183 on planes 16, 17, 48 and 49, are version 5.2, same as in the Near Detector. The Near Detector  
184 FEBs are designed to read out data in a fester rate and we used a mix of FEB types to study the  
185 difference in their response and to validate both versions in the same environment [15].

## 186 **Environment**

187 Unlike the near and the far detector, the Test Beam detector does not have any overburden to  
188 shield it from cosmic particles.

189 Temperature very stable during winter months (heaCng is installed at MC7). However, dew  
190 point went over 10C ND shutdown threshold several times.

## 191 **Underfilled cells issue**

192 The Test Beam detector is slightly tilted around the Z axis by about 0.7° towards the readout.  
193 This caused the top cells of both modules of all the horizontal planes (cells 31 and 63) to be

underfilled, creating an air bubble on the left side of the detector and severly affecting the energy response in those cells [15]. This has been fixed [16] by adding extensions to the filling ports and overfilling the horizontal cells with the NDOS scintillator stored in drums Fermilab (not the scintillator store in a tanker or tanks). This scintillator was also used in the first half of the detector (Fermilab ND+NDOS oil on figure 2), but is different from the "Ash River oil" used in part of the second half of the detector (bright part of figure 2). The overfilling was done in April 2021 in 3 stages in between the full operation of the Test Beam detector.

### 3 NOvA calibration process

Test Beam is following the same ideas and procedures as the standard NOvA calibration. This section intends to provide only a brief overview of the NOvA calibration. Further details can be found in the other NOvA calibration technical notes [17].

The purpose of calibration is to make sure that we get the same amount of energy wherever or whenever it's deposited in whichever of NOvA's detectors and to express this energy in physical units. The NOvA calibration uses cosmic ray muons, which provide a consistent, abundant and well-understood source of energy deposition and consists of two closely connected parts [18]:

1. The **relative calibration** corrects for attenuation of scintillator light as it travels through the cell to the readout, as well as for differences between detector cells.
2. This is followed by the **absolute calibration**, which only uses stopping muons when they are minimum ionising particles and calculates a scale between the measured charge readout, corrected by the relative calibration, and the simulated energy deposition in physical units of MeV. This scale is calculated for each time period and each detector separately, which ensures the energy deposition is directly comparable wherever or whenever it occurred.

There is also **timing calibration**, which corrects for the time differences of the signal to be processed and is done as a separate project to the relative and absolute calibrations and is out of scope of this technical note [19].

The units and variables used to define energy deposited in NOvA detectors are listed in table 2:

The final result of the NOvA calibration is the deposited energy in terms of physical units, which is in effect calculated as:

$$\begin{aligned}
 E_{dep}[\text{MeV}] = & \underbrace{\frac{\text{MEU}_{truth}[\text{MeV}/\text{cm}]}{\text{MEU}_{reco}[\text{PECorr}/\text{cm}]}}_{\substack{\text{Absolute calibration} \\ (\text{Detector, epoch})}} \times \underbrace{\frac{\text{Average response}[\text{PECorr}]}{\text{Fitted response}[\text{PE}]}}_{\substack{\text{Relative calibration} \\ (\text{Detector, epoch, plane, cell, w})}} \times \underbrace{\left[ \frac{\text{PE}}{\text{ADC}} \right]}_{\substack{\text{Scale} \\ (\text{APD Gain, FEB})}} \times \text{Signal}[\text{ADC}],
 \end{aligned} \tag{1}$$

where both the relative calibration results (blue fraction) and the absolute calibration results (red fraction) are stored in a database and applied together with the ADC-to-PE scale by the NOvASoft *Calibrator* package during processing of every hit in the NOvA detectors.

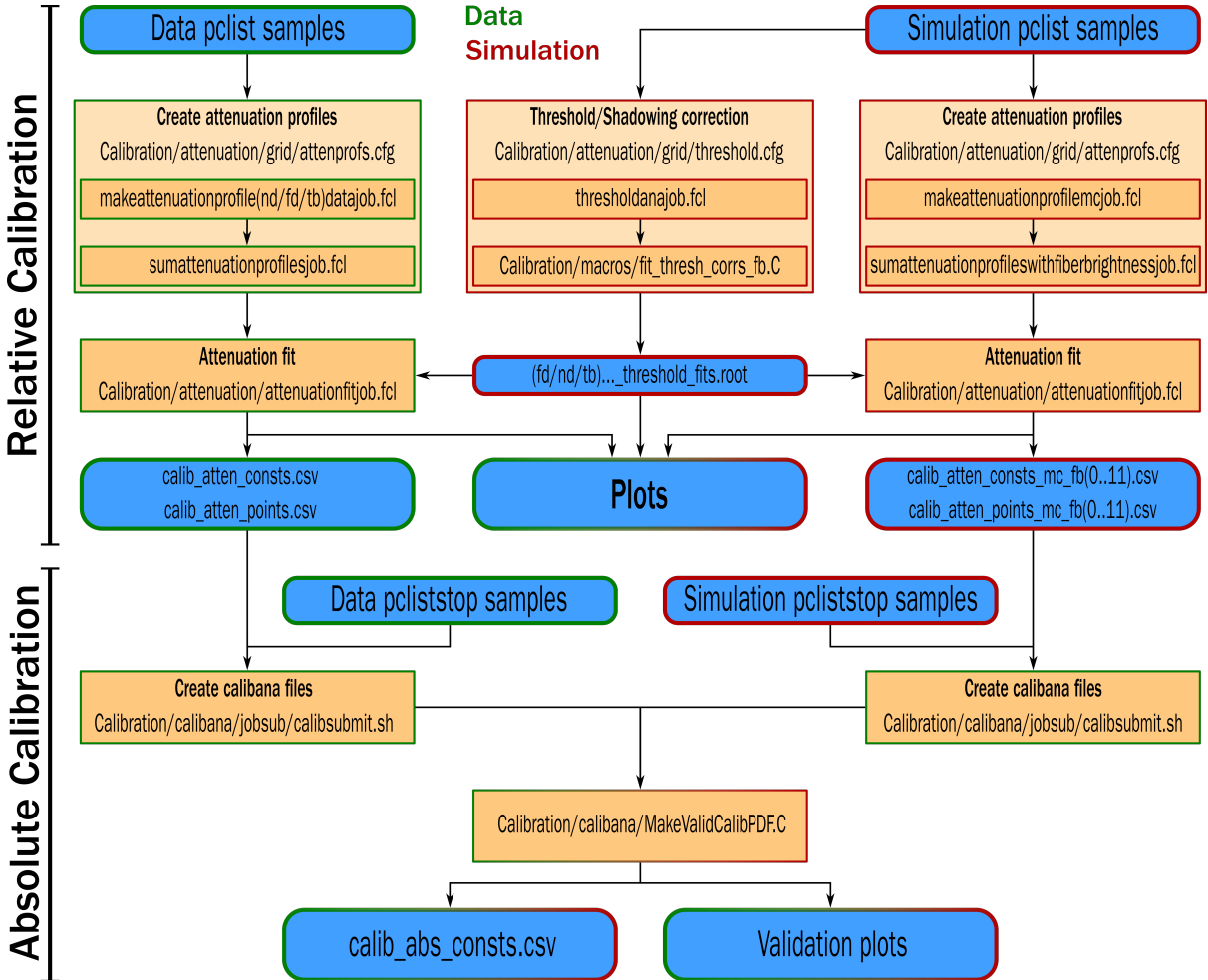


Figure 3: Flow chart showing the jobs (orange background) and files (blue background) needed and produced during the full NOvA calibration process. The left chain is showing the data calibration process (with green border) and is applied to every data calibration sample separately (periods or epochs). The center and right chains are showing the simulation calibration proces (red border), which is redone only if there's a change to the detector simulation. The absolute calibration at the bottom combines data and simulation. The entire process is done separately for each NOvA detector.

ADC	The digitized charge collected by the APDs from the Analog to Digital Converter [20].
PE	Number of Photo Electrons. Calculated by a simple rescaling of the best estimate of the peak ADC. The PE per ADC scale only depends on the FEB type and the APD gain settings. This is technically done before the calibration and serves as the base unit for calibration.
PECorr	Corrected PE after applying the relative calibration results. The correction is a ratio between an average energy response (a pre-determined semi-arbitrary number) and the result of the the relative calibration fit (also called attenuation fit), which depends on w, cell, plane, epoch and detector. This makes the energy response equivalent across each detector.
MEU	Muon Energy Unit is the mean detector response to a stopping cosmic minimum ionising muon. Mean MeV/cm or mean PECorr/cm
MeV	Estimated energy deposited in the scintillator calculated from PECorr using the results of the absolute calibration. Additional correction for dead material needs to be made in order to get a calorimetric energy estimate.

Table 2: Definitions of variables commonly used in calibration [17, 18].

## 226 Creating calibration samples

227 To select good quality cosmic ray muons we first remove beam related events based on their  
 228 time stamp relative to the time of the beam spill, as shown on figure 4. Then we apply basic  
 229 reconstruction and track-based selection.

230 Since energy deposition in a cell depends on the pathlength the particle traveled through  
 231 the cell, we only use hits for which we can reliably calculate their pathlength. We call these  
 232 hits **tricell** hits, as we require that all accepted hits also have a recorded hit in both neighboring  
 233 cells of the same plane, as shown on figure 5. In case there's a bad channel in a neighboring  
 234 cell, we ignore this channel and look one cell further. We can then calculate the pathlength  
 235 simply as the cell width divided by the cosine of the direction angle [17, 18].

236 For the absolute calibration we select muons that stop in the detector. For this we identify  
 237 muons with a Michel electron at the end of their track and only selection those [21].

238 For each data period/epoch and each simulation version we create two calibration samples  
 239 that are used as the input for the relative and absolute calibration. The samples are called [22]

- 240 • **pclist** = **list** of **pre**-calibrated hist; Contains all selected cosmic muon events and is used  
 241 in the relative calibration;
- 242 • **pcliststop** = **pclist** files only containing stopping muons used for the absolute calibration

## 243 Fiber brightness

244 For data, the relative calibration is done for each individual cell in each plane to properly  
 245 account for any potential variations. Therefore we have to repeat the attenuation fit  $N_{cell} \times$   
 246  $N_{plane}$  times. However, generating enough simulated events would be very computationally

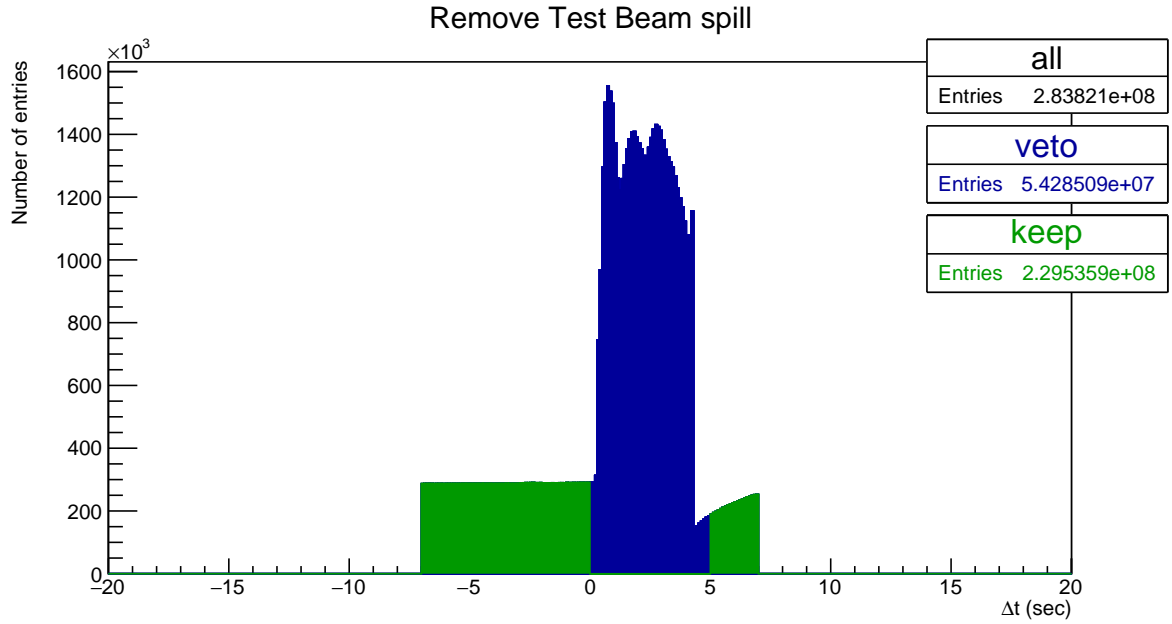


Figure 4: Test Beam beam spill events removed from the calibration samples. Test Beam beam spill is 4.2 seconds long and we remove events (in blue) within a 5 seconds window from the start of the beam spill. The remaining events (green) should mostly consist of cosmic particles. This example and the numbers of entries are for the full period 4 Test Beam sample.

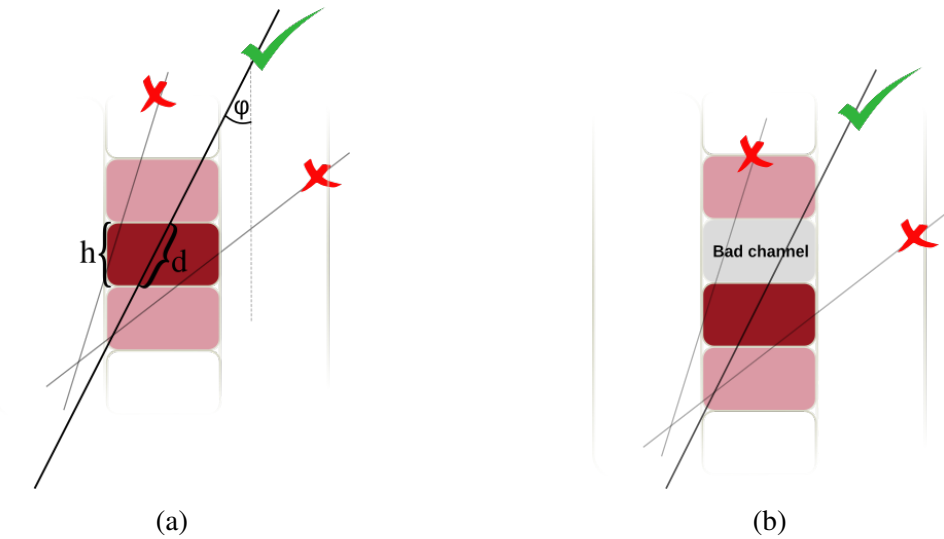


Figure 5: Illustration of the tricell condition (a). We only use hits that have two surrounding hits in the same plane to be used in the NOvA calibration. This is to ensure a good quality of the pathlength ( $d$ ) reconstruction, which is calculated from the known cell height ( $h$ ) and the reconstructed track angle ( $\phi$ ). In case the hit is next to a bad channel (b), we ignore this bad channel and require a hit in the next cell over.

intensive. Additionally, we can assume that the simulated detector is approximately uniform plane to plane. Therefore, for simulation, we want to *consolidate* the detector planes and only consider variation in the two views and their cells, so repeat the fit  $N_{cell} \times N_{view}$  times [23, 24].

There are some variations in the detector response cell by cell, that can be caused by different fiber brightnesses, but also by different qualities of the scintillator, air bubbles, APD gains, looped or zipped fibers and potentially others. To emulate these differences in the simulation without the need to simulate every cell individually and properly, we divide all the cells of each detector into 12 brightness bins, as shown on figure 6. These bins describe the relative differences in the detector response between individual cells [24]. Therefore in the end, for simulation we perform the attenuation fit in the  $N_{view} \times N_{fiberbrightnessbin} \times N_{cell}$  phase space.

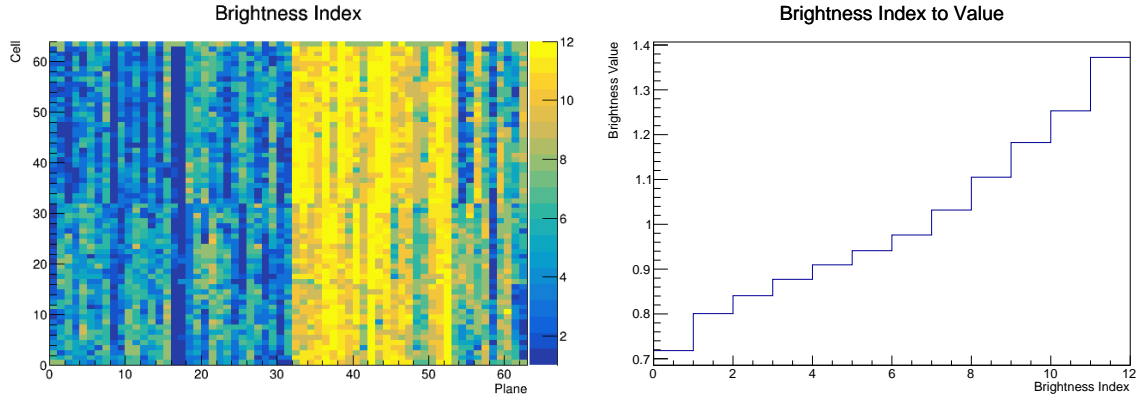


Figure 6: The Test Beam detector is (like the standard NOvA detectors) divided into 12 brightness bins (left plot), each representing a relative difference in energy response (right plot) due to different brightnesses of the fibers, scintillators, or readout.

## Threshold and shielding correction

Energy deposited far away from the readout may get attenuated enough to be shifted below the threshold. These low energy depositions would be missing from the attenuation fit, biasing it towards larger light levels going away from the readout. A similar effect, specifically for the vertical cells, is caused by using cosmic muons for calibration. The top of the detector effectively shields the bottom of the detector, skewing the energy distribution of cosmic muons. To correct for both of these effects, we use simulation to calculate the threshold and shielding (also called threshold and shadowing) correction by comparing the true and reconstructed information. We apply this correction before the attenuation fits [23].

### 3.1 Relative calibration

Relative calibration aims to create a fit, called *attenuation fit*, to the detector response over the position in a cell separately for every cell inside each detector. Scaling the fitted response to match the "average response" of the detector effectively removes relative differences throughout and between all cells across the entire detector. This average response is a single number chosen to approximately represent the average response in the middle of the cell. For the Far Detector this number is 39.91 PE, for the Near Detector it's 37.51 and for Test Beam it's the

273 same as for the Far Detector 39.91. The scale of this number has no impact of this result as the  
274 absolute scale of the detector response is determined during the absolute calibration [18, 23].

275 To create the attenuation fit we follow the following procedure [18]:

276 1. Create *attenuation profiles*, which are profile histograms of detector response in terms of  
277 energy deposited per pathlength (PE/cm) as a function of position in the cell ( $w$ ) through  
278 each cell for all planes. We construct the attenuation profiles over a little wider range  
279 than the actual length of the cell and always with 100 bins for each detector. This means  
280 that smaller detectors, like the Test Beam detector, have a finer binning ( $\sim 3\text{cm/bin}$ )  
281 compared to the Far Detector ( $\sim 18\text{cm/bin}$ ).

282 2. Analyse the attenuation profiles. The job to create the attenuation profiles also creates  
283 validation histograms, which should be analyzed prior to performing the attenuation fit  
284 to make sure the attenuation profiles look as expected.

285 3. Apply the threshold and shielding correction that were created using the simulation plist  
286 sample before the relative calibration.

287 4. Do the attenuation fit over the full length of each cell. The fit consists of

288 (a) exponential fit, which combines two cases. Light from the energy deposition travelling  
289 straight to the readout, or going the opposite direction, looping around the cell  
and then to the readout. The fitted function has a form:

$$y = C + A \left( \exp\left(\frac{w}{X}\right) + \exp\left(-\frac{L+w}{X}\right) \right), \quad (2)$$

288 where  $y$  is the response,  $L$  is the length of the cell and  $C$ ,  $A$  and  $X$  are the fitted  
289 parameters.  $X$  also represents the attenuation length.

290 (b) To remove the effect of residuals, mainly at the end of cells, we smooth out the  
291 residuals from the exponential fit with LOcally WEighted Scatter plot Smoothing  
292 (LOWESS).

293 5. Check the plots of the attenuation fit for a selection of cells.

294 6. Save the fit result to the database in the form of two csv tables. The *calib\_atten\_consts.csv*  
295 table holds the results of the exponential fit, together with the final  $\chi^2$  of the fit. The  
296 *calib\_atten\_points.csv* table holds the results of the LOWESS smoothing.

297 To ensure the quality of the attenuation fit, we only apply the results if the final  $\chi^2 < 0.2$ .  
298 If  $\chi^2 > 0.2$  we ignore the results for this cell and mark it as *uncalibrated*.

## 299 3.2 Absolute calibration

300 To find the absolute energy scale, we apply the relative calibration results on the stopping muon  
301 sample and look at the energy they deposited in cells 1-2 meters from the end of their tracks.  
302 In this track window they are minimum ionising particles and their energy deposition is almost  
303 constant and well understood. We take a mean of their corrected deposited energy separate for  
304 each view and for each calibrated sample. We then take the average over the two views to get  
305 the final  $\text{MEU}_{\text{reco}}/\text{PECorr}/\text{cm}$  for each sample [21].

306 From simulation we get the mean of the true energy deposited in scintillator  $\text{MEU}_{truth}\text{MeV}/\text{cm}$   
307 for the same sample of stopping muons. We ignore the energy that's lost in the dead material  
308 (PVC extrusions) and deal with it separately. The absolute energy scale for each sample is then  
309 the ratio of  $\text{MEU}_{truth}/\text{MEU}_{reco}$ . We save these absolute energy scales in another csv table called  
310 *calib\_abs\_consts.csv* which stores the MEU values and their errors.

311 As part of the absolute calibration we also produce validation plots that show the effect of  
312 calibration on the distribution of the stopping muons. We analyse these plots and if everything  
313 looks all right load all the csv tables into the database.

### 314 **3.3 Calibration uncertainties**

#### 315 WORK IN PROGRESS

## 316 **4 NOvA Test Beam detector calibration**

### 317 **4.1 Overview**

318 Adding the underfilled cells to the bad channels which are automatically skipped for the tricell  
319 condition

320 Period naming, possibly epochs (for P3). List of data samples, plus MC samples that were  
321 used and pointer to the data-based simulation technote.

322 Specific running conditions: - maybe enough to mention this in the individual descriptions  
323 of the test beam periods Underfilled cells Faulty FEBs (Period 2 and Period 3)

324 Why do we do the calibration generally and why do we need to do in for Test Beam specif-  
325 ically - probably in the introduction

326 Temperature study (small overview - probably not needed at all, depends if Randeeth want  
327 to add his work to this technote)

328 From Teresa's thesis Along with setting the energy scale of the detector, we need to calibrate  
329 the timing of the readout system for the detector. The Data Concentrator Modules (DCMs)  
330 responsible for collating the data from multiple FEBs get their timing information via a daisy  
331 chain originating at the detector TDU. Each DCM in the chain has a timing offset relative to the  
332 DCM before it, with the last DCM having the earliest ti. Following the procedure described in  
333 [66], I used timing information from hits on cosmic ray muon tracks that pass through multiple  
334 DCMs to determine the relative offsets between DCMs, shown in Figure 3.20.

#### 335 **4.1.1 Definitions**

336 List all final data and simulation definitions used.

337 Mention exactly the name and the location of the fcl files to create the TB plist/ppliststop  
338 files.

339 When were these files produced? Mention that we had to reprocess most of the files in 2023  
340 due to the changed geometry.

341 From Teresa's thesis: "For Test Beam, we have three beam-based triggers, one pulsed trig-  
342 ger, and two data-driven triggers. The data-driven triggers are both activity-based triggers. The  
343 first is intended to record cosmic ray induced events for use in calibrating the detector.

---

## pclist samples

---

**Data period 2:**

```
prod_pclist_R23-04-05-testbeam-production.a_testbeam_ddactivity1_period2_v1
```

**Data period 3:**

```
prod_pclist_R23-04-05-testbeam-production.a_testbeam_ddactivity1_epoch3a_v1
```

```
prod_pclist_R23-04-05-testbeam-production.a_testbeam_ddactivity1_epoch3b_v1
```

```
prod_pclist_R23-04-05-testbeam-production.a_testbeam_ddactivity1_epoch3c_v1
```

```
pclist_testbeam_detector_activity_epoch3d_R21-01-28-testbeam-production.a
```

```
pclist_testbeam_detector_activity_epoch3e_R21-01-28-testbeam-production.a
```

**Data period 4:**

```
prod_pclist_R23-04-05-testbeam-production.a_testbeam_ddactivity1_period4_v1
```

**Simulation:**

```
rkrilik_pclist_testbeam_databasedsim_R23-04-05-testbeam-production.a
```

---

## pcliststop samples

---

**Data period 2:**

```
prod_pcliststop_R23-04-05-testbeam-production.a_testbeam_ddactivity1_period2_v1
```

**Data period 3:**

```
prod_pcliststop_R23-04-05-testbeam-production.a_testbeam_ddactivity1_epoch3a_v1
```

```
prod_pcliststop_R23-04-05-testbeam-production.a_testbeam_ddactivity1_epoch3b_v1
```

```
prod_pcliststop_R23-04-05-testbeam-production.a_testbeam_ddactivity1_epoch3c_v1
```

```
pcliststop_testbeam_detector_activity_epoch3d_R21-01-28-testbeam-production.a
```

```
pcliststop_testbeam_detector_activity_epoch3e_R21-01-28-testbeam-production.a
```

**Data period 4:**

```
prod_pcliststop_R23-04-05-testbeam-production.a_testbeam_ddactivity1_period4_v1
```

**Simulation:**

```
rkrilik_pcliststop_testbeam_databasedsim_R23-04-05-testbeam-production.a
```

---

Table 3: SAMWEB definitions of the Test Beam calibration samples.

## <sup>344</sup> 4.2 Fiber Brightness

<sup>345</sup> To divide the Test Beam detector into fiber brightness bins we used the attenuation fit results  
<sup>346</sup> for period 4 data (described in section 4.8), since that is the best detector conditions data we  
<sup>347</sup> have.

<sup>348</sup> Describe and show plots that since we are only using the fitted response at cell centre we  
<sup>349</sup> can allow fits with  $\chi^2 > 0.2$ . Show examples of responses with chisq larger than that and say  
<sup>350</sup> what is the final chisq chosen. No need to show the final distribution of the fb bins here as they  
<sup>351</sup> were technically shown in the general calibration description. But might refer back to it...

## <sup>352</sup> 4.3 Simulation

<sup>353</sup> Should I talk about the "history" of the simulation of cosmics here, or in the introduction, or  
<sup>354</sup> not at all?

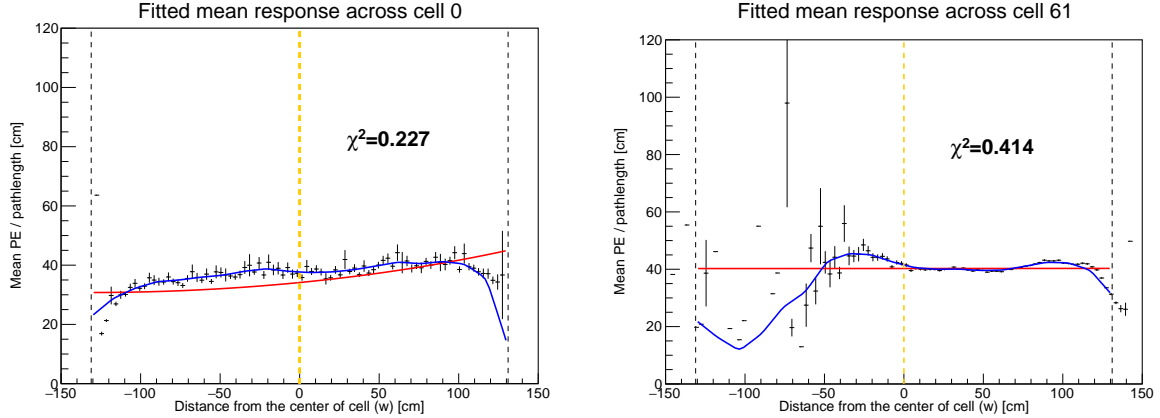


Figure 7: The Test Beam detector is (like the standard NOvA detectors) divided into 12 brightness bins (left plot), each representing a relative difference in energy response (right plot) due to different brightnesses of the fibers, scintillators, or readout.

355 We used a data-based simulation of cosmic muons for the Test Beam detector calibration.  
 356 The details are described in the Data-based simulation of cosmic muons (not only) for calibra-  
 357 tion technote [link to docdb]. We used half of period 4 data (used every second event as saved  
 358 in the root file, therefore sampled from the entire period 4) as inputs and the newly created fiber  
 359 brightness file to inform the simulation on the realistic detector conditions.

360 The distribution of events cosmic muon events from the new simulation is shown on figure  
 361 8.

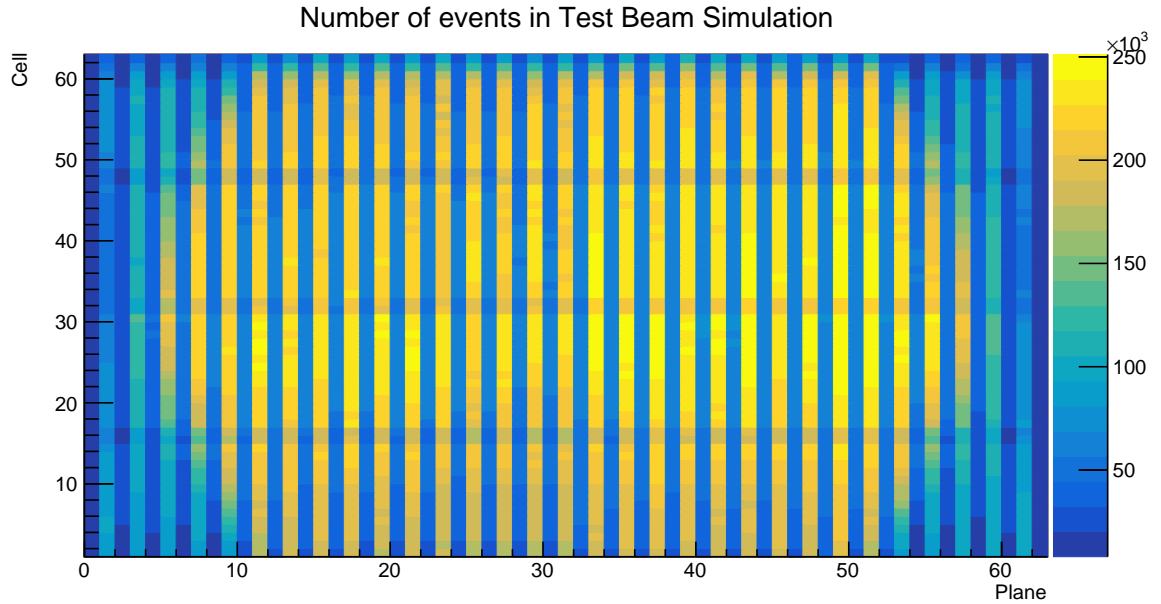


Figure 8: Distribution of events in the Test Beam simulation calibration sample.

362 The results of the attenuation fit are shown for each cell (in its centre) on figure 9. The  
 363 blank cells show which cells failed the attenuation fit (their  $\chi^2 > 0.2$ ). Most of the uncalibrated  
 364 cells are on the edges of the detector, which is expected as those have much fewer events that

365 pass our selection than the rest. Examples of a standard detector response and of the response  
366 for cells on the edge of the detector are shown of figure 10.

367 (I should explain here what is on the plots maybe - red is the exponential fit and blue is the  
368 total with with the LOWESS. Most cells have the expected response of slow rise towards the  
369 readout falling down on the edges).

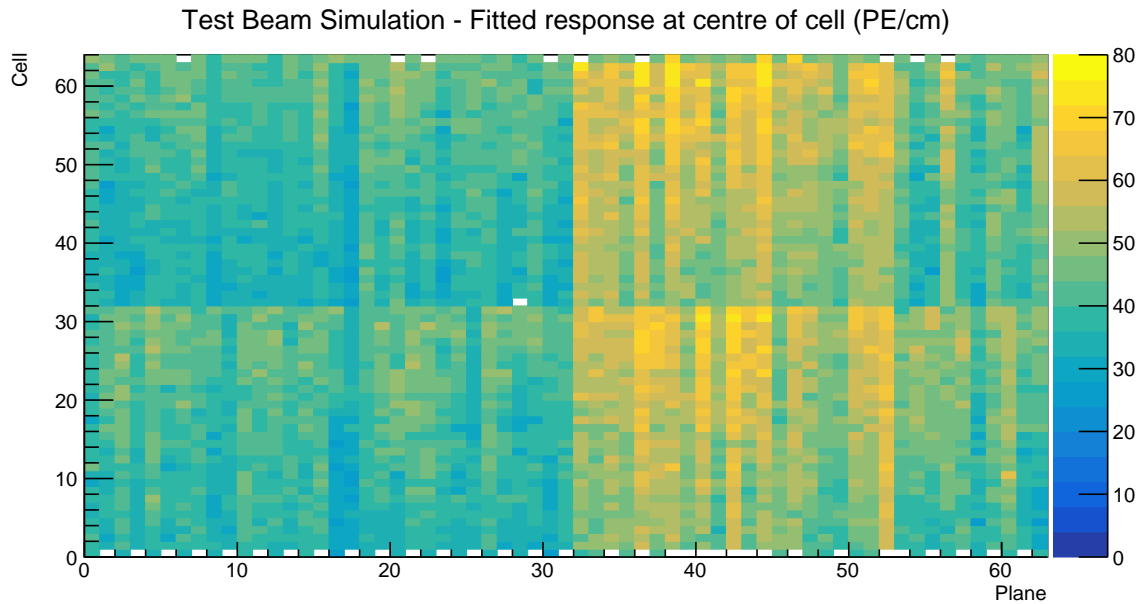


Figure 9: Overview of the attenuation fit results for the Teast Beam detector calibration simulation. Each cell represents the result fo the attenuation fit to the energy response in the centre of that cell. The blank cells are uncalibrated.

370 There is only one cell in the middle of the detector that is left uncalibrated, which is the cell  
371 32 in a vertical plane in the brightness bin 5, shown on the top right of fig.10. The corresponding  
372  $\chi^2 = 0.227$ . It seems the reason the  $\chi^2 > 0.2$  is an exceptionally high response with a large  
373 uncertainty in the last bin.

374 This is a much better result of the relative calibration (attenuation fit) for a simulation than  
375 the previous versions of Test Beam detector calibration simulations were able to accomplish.

#### 376 4.4 Threshold and shielding corrections

377 The threshold and shielding correction for Test Beam is almost uniform across all cells as can  
378 be seen on figure 11. This is expected as the hight of the Test Beam detector is 2.6 m has only  
379 a negligible effect on the energy distribution of cosmic muons or on the threshold saturation.  
380 The correction is basically just a normalization factor, except for the cell edges, but there is a  
381 large variation in the energy response there anyway due to low number of events. Since the  
382 relative calibration only cares about relative differences across the detector, a normalization  
383 factor doesn't change anything.

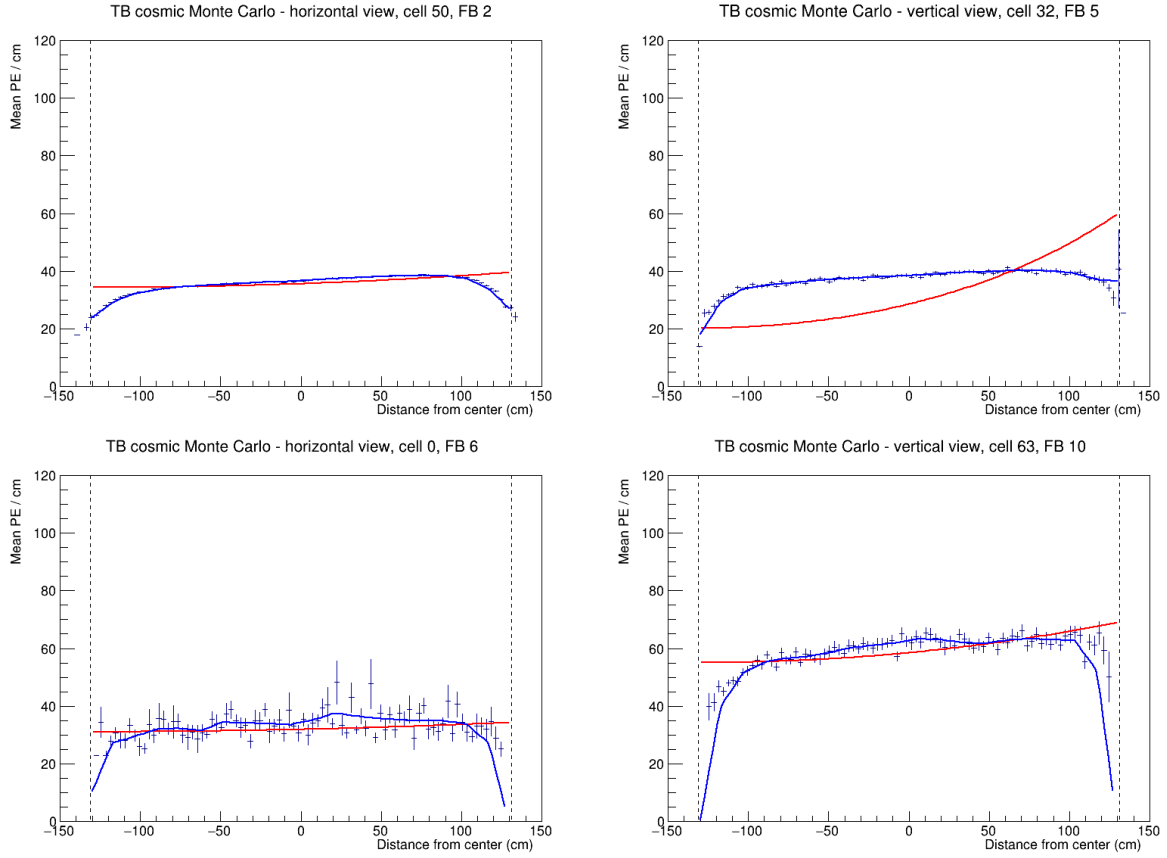


Figure 10: Attenuation fits for a selection of cells in the Test Beam calibration simulation. Top left is an example of a successful attenuation fit, top right is a failed fit due to statistical fluctuation in the last bin and the bottom plots show failed fits for cells on the edges of the detector.

## 384 4.5 Period 1

385 Only a month of data, only first half of detector filled, primary/secondary beam halo, or over-  
 386 saturation leading to FEB shutoffs [docdb:38349 and 41331]. Only used for commissioning, not  
 387 used for any data analysis or calibration.

## 388 4.6 Period 2

389 The underfilled cells issue described in section 2 was present throughout period 2 data taking.  
 390 This can be clearly seen on figure 12, represented by the empty cells 31 and 63 in the horizontal  
 391 planes, which were marked as bad channels and therefore ignored during processing. This also  
 392 affects the neighboring cells to the underfilled cells, which have fewer events due to the tricell  
 393 condition.

394 There was also an issue of switched cables from the readout in plane 55 between cells 3  
 395 and 46 [25], which can also be seen on figure 12. This is manifested as fewer total number of  
 396 events in those cells and in their neighbours, again due to the tricell condition.

397 Officially, period 2 is divided into 6 epochs 2a - 2f, compared on figures 13, 14 and 15. The  
 398 epochs mostly differ in the use of various FEB firmwares, with epoch 2c being a trigger study

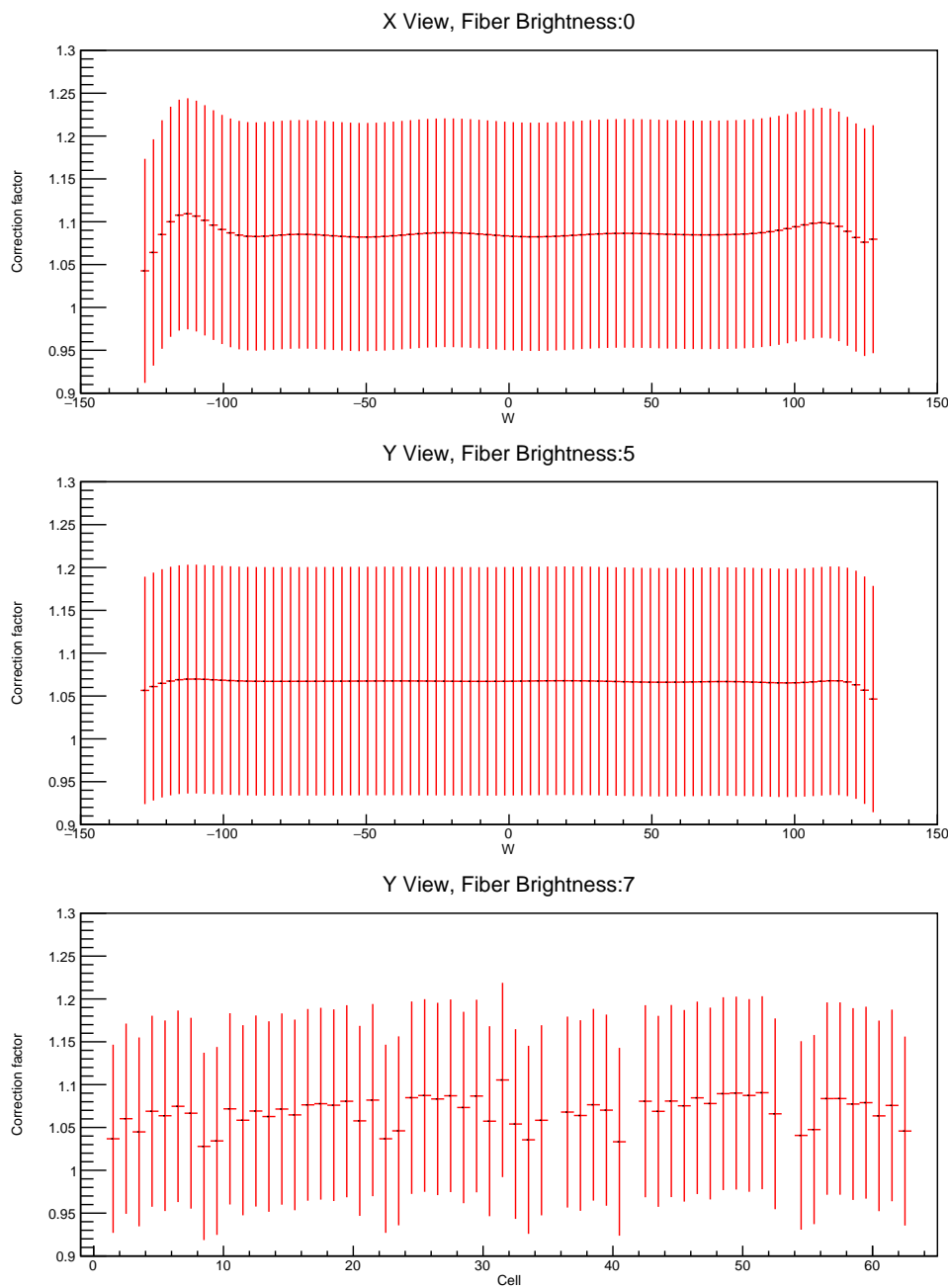


Figure 11: Examples of threshold and shielding corrections for the Test Beam detector

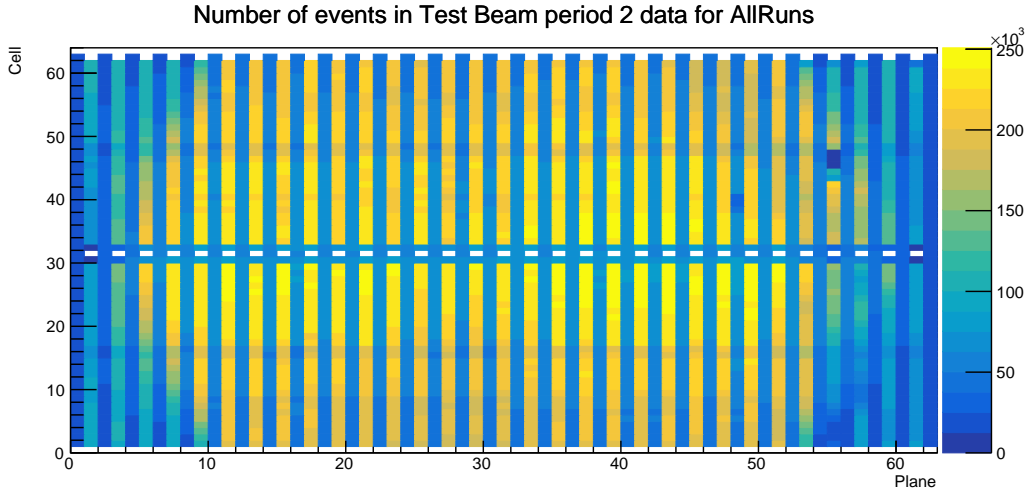


Figure 12: Distribution of events in the period 2 Test Beam data calibration sample.

399 with paddles. As can be seen on the plots, the individual epochs vary only slightly, only in a  
 400 small normalization. We decided to use the entire period 2 without splitting it into any smaller  
 401 samples for calibration.

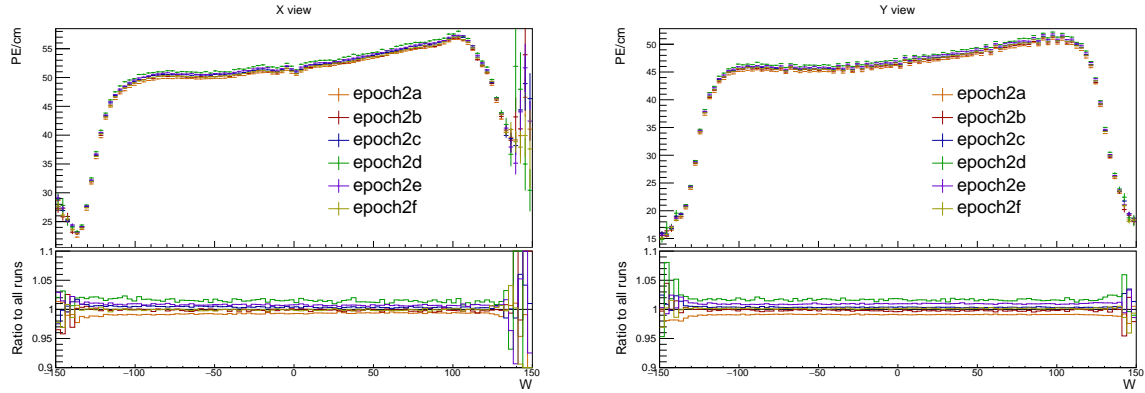


Figure 13: Uncorrected average energy response as a function of the position within a cell ( $w$ ) for epochs in period 2. It is clear that there is no significant difference between the various epochs.

## 402 Period 2 relative calibration results

403 The results of the attenuation fit for period 2 are summarised on figure 16 showing the fitted  
 404 response at the centre of each cell, or blank cell if the cell failed calibration.

405 Most of the cells have the expected response, as shown on the left plot of figure 17. Here  
 406 the mean response in PE/cm slowly and approximately constantly rises towards the readout  
 407 (right side of the plot) and drops down on the cell edges, marked with dashed lines.

408 Some cells have a non-flat response across the cell, with one or more regions with lower en-  
 409 ergy response, as shown on the right plot of figure 17. These low regions are (almost certainly)  
 410 a real physical effect caused by zipped, or possibly even twisted fibers [26], present in all of  
 411 NOvA's detectors. Relative calibration corrects for this effect in data, but zipped fibers are not

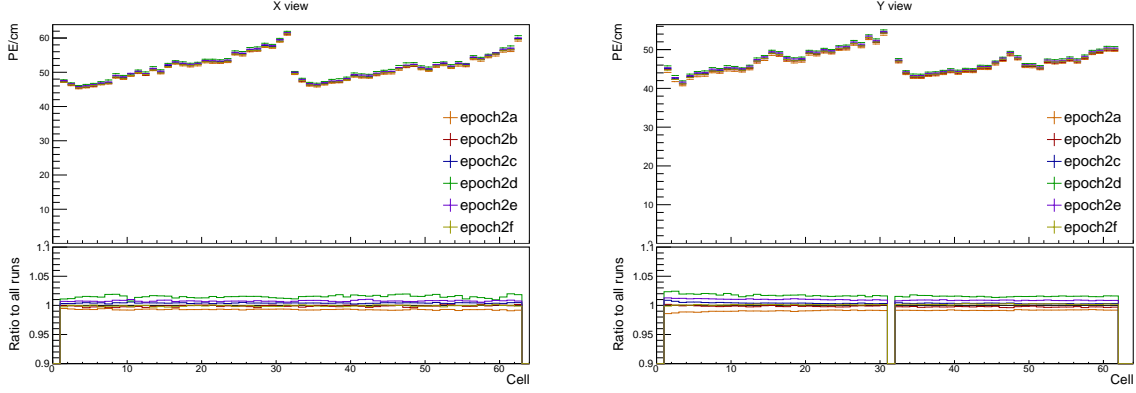


Figure 14: Uncorrected average energy response as a function of cells for epochs in period 2.

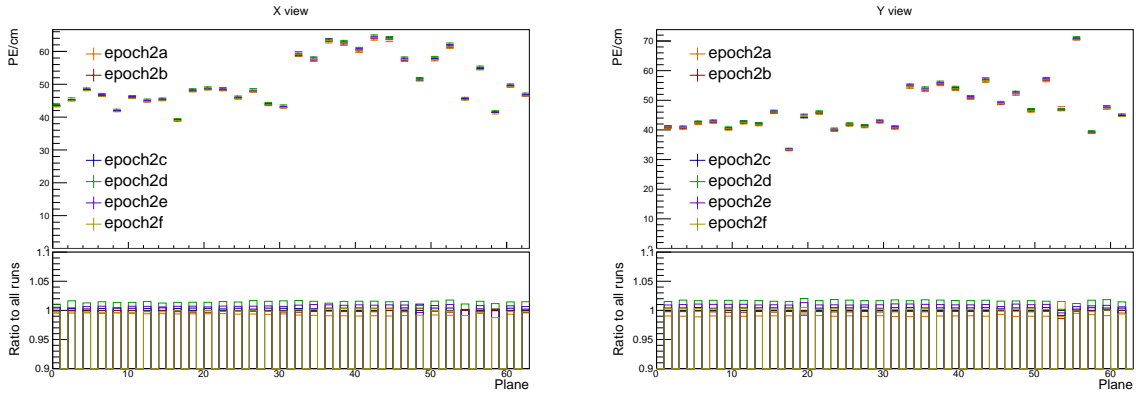


Figure 15: Uncorrected average energy response as a function of planes for epochs in period 2.

412 included in simulation, for any of the detectors. This could potentially cause issues with the  
413 ADC threshold in simulation.

414 Since the underfilled cells were marked as bad channels we didn't even attempt to calibrate  
415 them. Their neighbours have fewer events due to the tricell condition but majority of them  
416 pass the calibration condition, as shown on figure 18. The neighbouring cells in plane 1 don't  
417 pass the calibration due to low statistics and therefore large fluctuations, as shown on figure 19.  
418 This is likely due to a combination of the tricell condition and plane 1 being on the edge of the  
419 detector, which typically has fewer (accepted) hits than the center as shown on figure 12.

420 The left half of plane 55 has  $> 3 \times$  larger response than it's surrounding planes, as shown  
421 on the left plot of figure 20. Similarly, the left half of plane 57 has lightly lower response than  
422 the surrounding planes, as shown on the right plot of figure 20. This is due to the corresponding  
423 APDs/FEBs faultily recording different energy response than the real energy deposited in the  
424 detector. Since this is present for all data, not only for the comsic muons used for calibration, it  
425 is important to correctly calibrate them. The issue can arrise if these FEBs have been "faulty"  
426 only for a limited time of the entire calibrated period. Since we are doing the attenuation fit on  
427 the profile histograms, if an FEB records a standard response for half of the time and  $7 \times$  larger  
428 response for the seconds half, calibration is going to assume the response was  $4 \times$  larger the  
429 entire time, which is incorrect. Since both of these planes are in the back of the detector, we  
430 decided to ignore this effect for period 2.

431 The swapped cables in plane 55 have almost no events, which affects both them and their

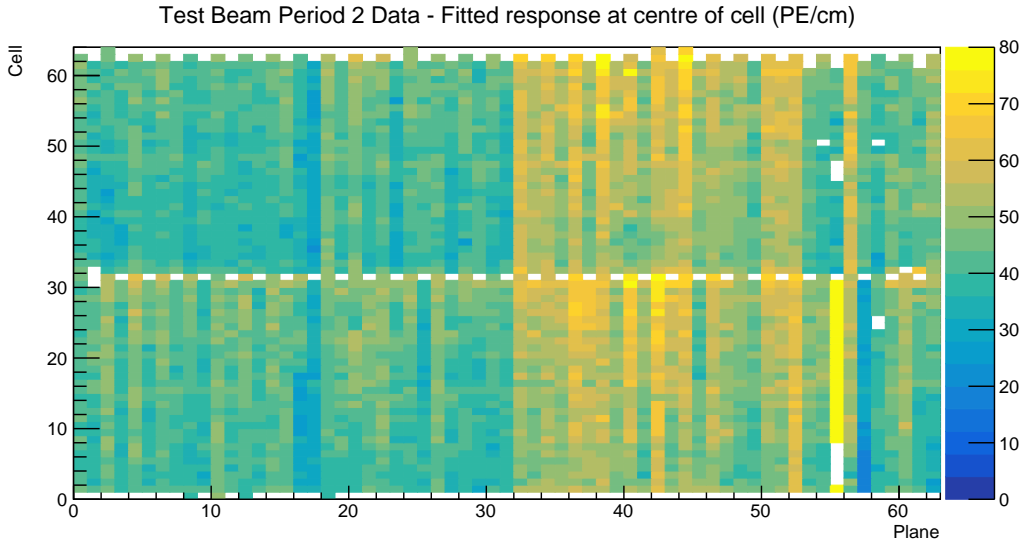


Figure 16: Overview of the relative calibration results for the Teast Beam detector period 2 data. Each cell represents the result of the attenuation fit to the energy response in the centre of that cell. The blank cells are uncalibrated.

<sup>432</sup> neighbours as shown of figure 21.

<sup>433</sup> Several cells in the end of the Test Beam detector are uncalibrated due to bins on the edges  
<sup>434</sup> of the cell having an unusually high response, or no events at all, as shown on figure 22. It is  
<sup>435</sup> unknown if this is a real physical effect, possibly related to the fibers, or unfiltered noise hits,  
<sup>436</sup> or something else entirely. Since these cells are in the end of the detector, it is safe to ignore  
<sup>437</sup> them.

## <sup>438</sup> 4.7 Period 3

<sup>439</sup> The underfilled cells were refilled (or overfilled) during the period 3 data taking. This was the  
<sup>440</sup> main motivation for dividing period 3 into individual epochs as shown on table 4. One more  
<sup>441</sup> major event that could impact the Test Beam data is the replacement of several faulty FEBs,  
<sup>442</sup> which motivated the creation of epoch 3e.

Epoch 3a	January 12 <sup>th</sup> 2021	Underfilled cells
Epoch 3b	April 21 <sup>st</sup> 2021	Overfilling the back 9 horizontal planes and the 7th horizontal plane from the front
Epoch 3c	April 27 <sup>th</sup> 2021	Overfilling of the 15 front horizontal planes (except the 7th, which was already done) and the 14th horizontal plane
Epoch 3d	April 30 <sup>th</sup> 2021	Overfilling of the remaining 8 horizontal planes
Epoch 3e	May 12 <sup>th</sup> 2021	FEB swaps

Table 4: Test Beam period 3 epochs, their start dates and the reason for thir separation.

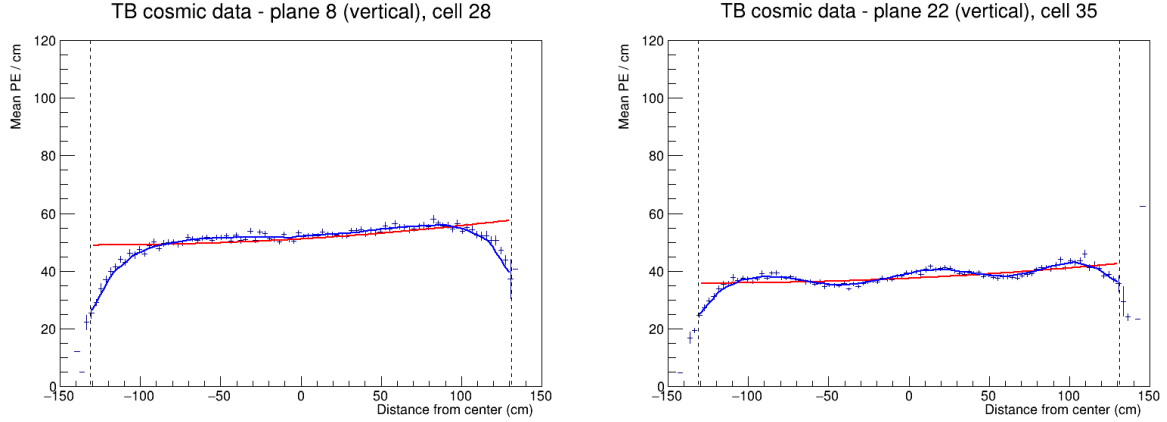


Figure 17: Attenuation fits for a selection of cells in period 2. Left plot shows an example of the standard energy deposition in the Test Beam. Right plot shows the effect of zipped fibers.

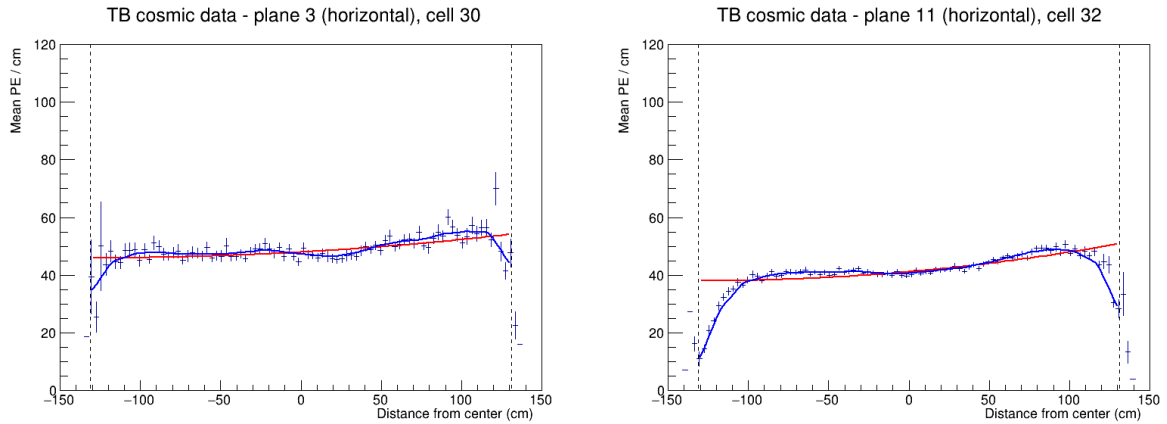


Figure 18: Fit to the energy response in period 2. The cells neighbouring the underfilled cells have fewer events and therefore larger fluctuations than the "usual" Test Beam cell.

443     The refilling of the underfilled cells can be clearly seen on the cell hits distribution on figure  
 444     23 and on the distribution of energy deposition across horizontal cells (Y view) on figure 25.

445     From the cell hits distributions we can also see there are a few channels (cells) that were  
 446     likely dead for a certain time and weren't recording the same number of events as the surround-  
 447     ing cells. This is specifically plane 48, cell 39 in all of period 3 and plane 18, cell 31 in epochs  
 448     3d and 3e.

449     The energy distributions across vertical cells and planes (X view) on figures 25 and 26  
 450     shows, that the top half of plane 58 has a very distinctly different energy deposition compared  
 451     to the rest of the cells, while having the same number of events, as can be seen on figure 23.  
 452     This is the most impactful of the faulty FEBs replaced for Epoch 3e.

453     From these discussion, we have decided to calibrate epochs 3a, 3b and 3c together (all  
 454     epochs containing any underfilled cells) and separately calibrated epochs 3d and 3e. The faulty  
 455     FEB in plane 58 is far enough in the back of the detector that we didn't find it necessary to  
 456     calibrate epochs 3d and 3e separately. Also epochs 3b and 3c only contain a few days worth of  
 457     data, which wouldn't be enough for a successful attenuation fit.

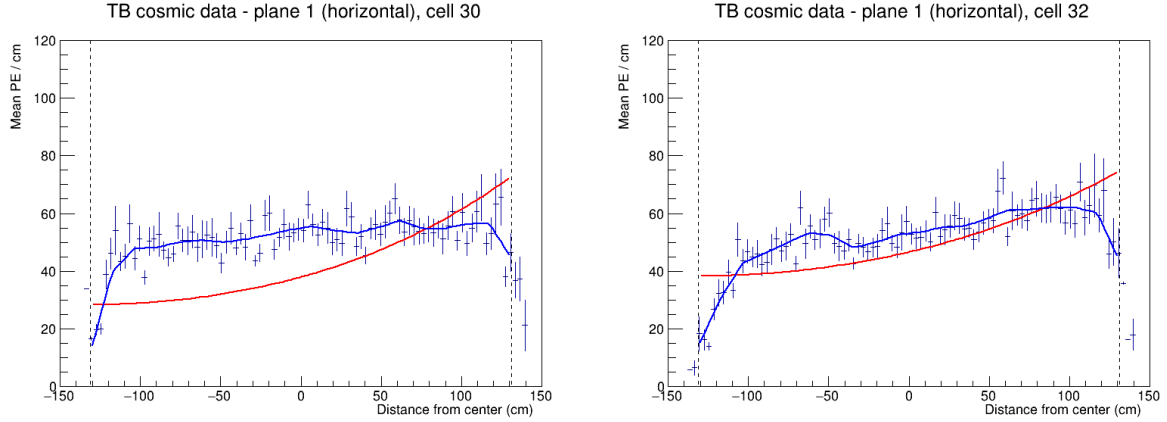


Figure 19: Fit to the energy response in period 2. The neighbouring cells to the underfilled cells in plane 1 are uncalibrated due to low statistics.

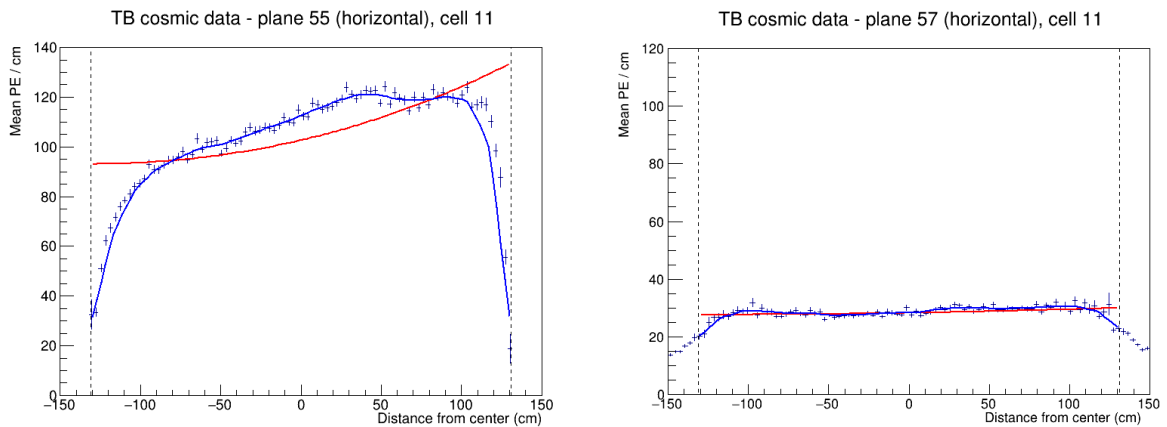


Figure 20: Fit to the energy response in period 2. Lower halfs of planes 55 and 57 have a different scale of energy response than the surrounding planes.

#### 458 Combined epochs 3a, 3b and 3c relative calibration results

459 The results of the attenuation fit are summarised on figure 27 showing cell  $\times$  plane distribution  
460 of the fitted response at the centre of each cell.

461 We can see that some of the underfilled cells that have been refilled for epochs 3b or 3c are  
462 now calibrated thanks to including them into the same attenuation fit. An example of energy  
463 deposition in such a cell is on the left plot of figure 28.

464 Same as in period 2 most of the neighbouring cells to the underfilled cells are calibrated,  
465 except for cell 32 in plane 1, shown on the right of figure 28, which is also affected by the low  
466 statistics at the edges of the detector.

467 There is a couple of notably faulty FEBs with a different energy response than their neigh-  
468 bours. Besides the expected top half of plane 58, which has about  $5\times$  larger response than the  
469 usual, it's also the top half of plane 36, which has about  $2.5\times$  larger response as its neighbours.  
470 This could mean that the FEB in plane 36 was faulty only for a limited time compared to the  
471 FEB in plane 58. The energy deposition for these cells is shown on figure 29.

472 Similarly as in period 2, there are a few cell in the back of the detector that have a sharp

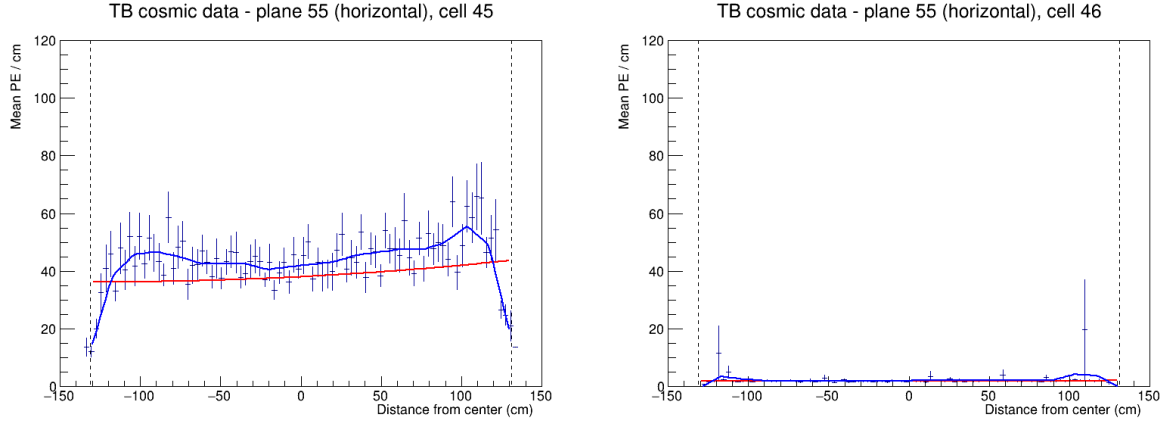


Figure 21: Fit to the energy response in period 2. Cells with swapped readout cables have almost no recorded events as shown on the right plot. This also affect their neighbouring cells due to the tricell condition as shown on the left plot.

473 rise in the energy response at the edge of the cell, which causes them to be uncalibrated. This  
474 can be seen on figure 30.

#### 475 Combined epochs 3d and 3e relative calibration results

476 The results of the attenuation fits for epochs 3 d and e are shown on figure 31. There we can  
477 see the expected uncalibrated cells in plane 17 related to the dead channel (or possible still  
478 underfilled cell). The energy deposition for this cell and one of its neighbours is shown on  
479 figure 32.

480 Epochs 3 d and e should have all the previously underfilled cells now refilled, but as can be  
481 seen on figure 31, there's several of these cells that are still uncalibrated. The energy deposition  
482 in these cells is shown on figure 33. We can see that these cells have a fairly large discrepancy  
483 between the left and right side of the cells. This is caused by using different scintillator oils for  
484 the initial filling of the cells and for the refilling. Specifically, these cells have been initially  
485 filled with the Ash River and the Texas oils, which have higher energy depositions compared  
486 to the NDOS oil that was used for the refilling. These oils clearly didn't mix properly which  
487 causes a different energy deposition in different parts of the cells. Since this is a physical effect  
488 that should be accounted for in the calibration and as we can see the fits are actually performing  
489 pretty well and are just confused by the unusual shape. We have therefore decided to manually  
490 change the  $\chi^2$  inside the cvs tables (results of the attenuation fits), so that the  $\chi^2 < 0.2$  and  
491 these cells are considered calibrated.

492 Some of the cells in the back of the detector have a rise, or drop in energy deposition at the  
493 edge of the cell, as can be seen on figure 34. This is similar to the effect seen in period 2 and  
494 epochs 3abc and since it's again concentrated in the end of the detector we ignored these cells  
495 and left them uncalibrated.

## 496 4.8 Period 4

497 The period 4 Test Beam data taking period is the best data we managed to collect with almost an  
498 ideal condition of the detector. There's only a few commissioning runs in the very beginning,

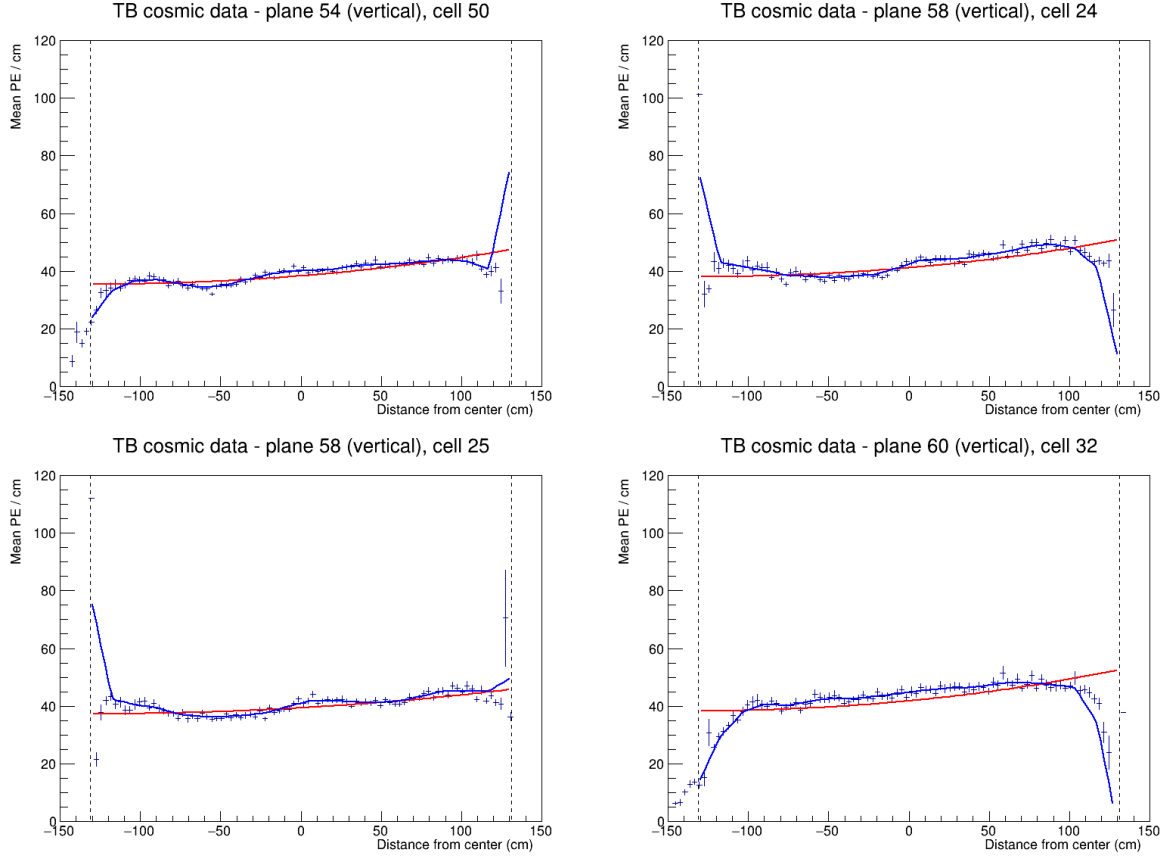


Figure 22: Fit to the energy response in period 2. Examples of cells that have an unusually high or low energy response at the edge of the cell. These cells are not calibrated.

499 which uncovered some dead channels or faulty FEBs that have been fixed. These runs make  
 500 epoch 4a shown on the top plot of figure 35.

501 There has also been a cell masking study [reference], during which we masked parts of the  
 502 front of the detector to help with FEB saturation. We can clearly see this on the middle plot of  
 503 figure 35.

504 Figures 36, 37 and 38 show that the epoch 4a and the cell masking study did have a notice-  
 505 able impact on the energy deposition across the detector. We have therefore decided to ignore  
 506 these runs and only use the rest of the period 4 data for the calibration.

## 507 Period 4 relative calibration results

508 Results of the attenuation fits for period 4 are summarised on figure 39.

509 We can see that majority of the detector is calibrated, besides some cells on the edge of the  
 510 detector, a few formerly underfilled cells (left plot on figure 40) and one cell with an unusually  
 511 high response at the edge of the cell (right plot on figure 40). We treated the formerly underfilled  
 512 cells the same way as in epochs 3 d and e, by manually changing their  $\chi^2$  to be  $< 0.2$  and  
 513 therefore making them calibrated.

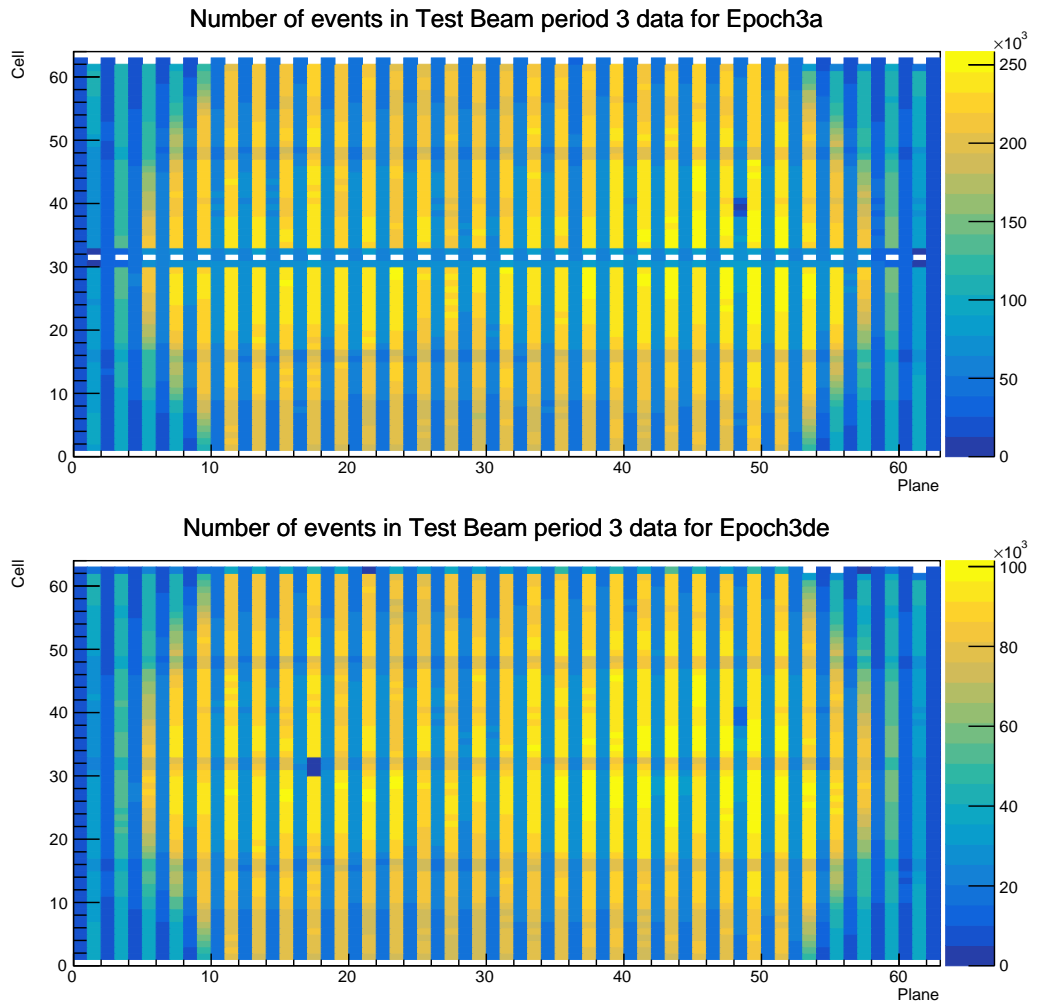


Figure 23: Distribution of events in the period 3 Test Beam data calibration sample. Comparison of Epoch 3a data before the refilling of the underfilled cells and Epoch 3de (combination of Epochs 3d and 3e) after the full refilling.

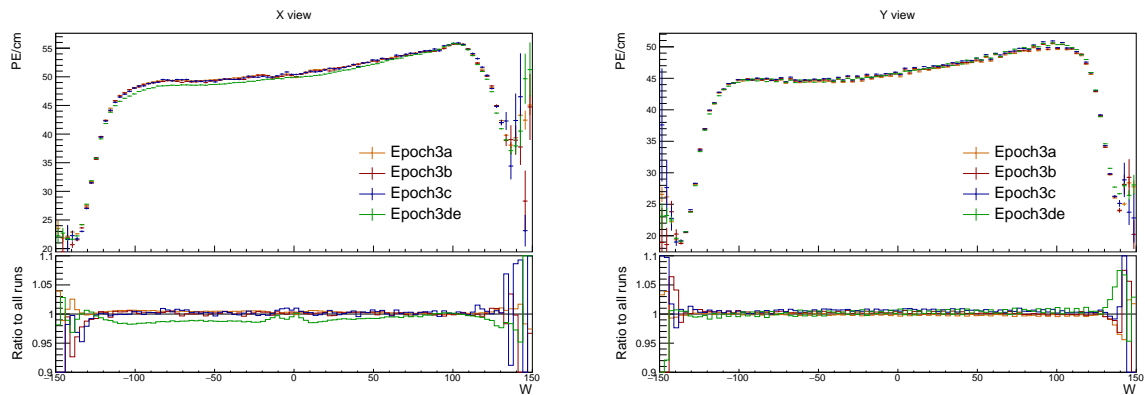


Figure 24: Uncorrected average energy response as a function of the position within a cell ( $w$ ) for epochs in period 3.

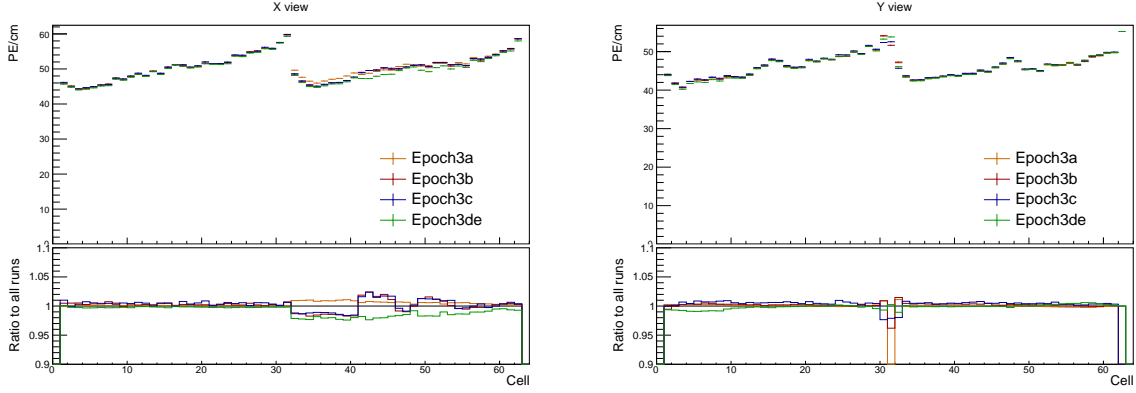


Figure 25: Uncorrected average energy response as a function of cells for epochs in period 3.

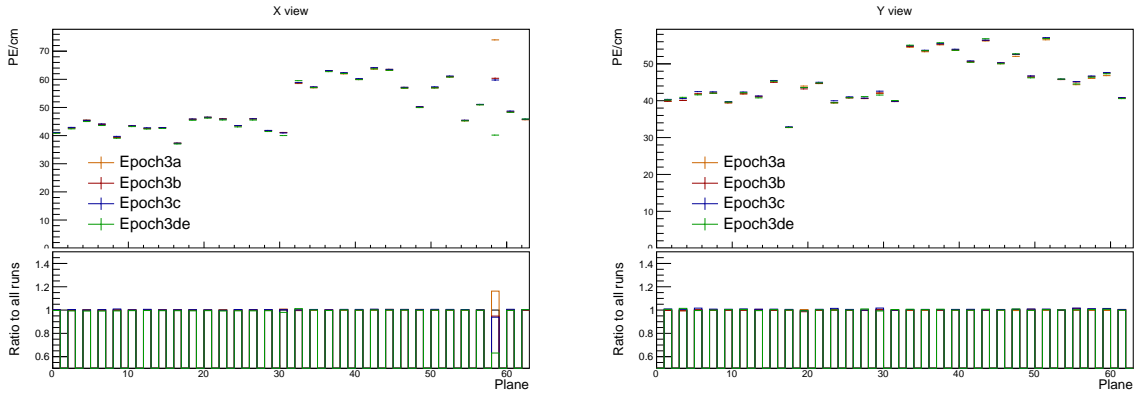


Figure 26: Uncorrected average energy response as a function of planes for epochs in period 3.

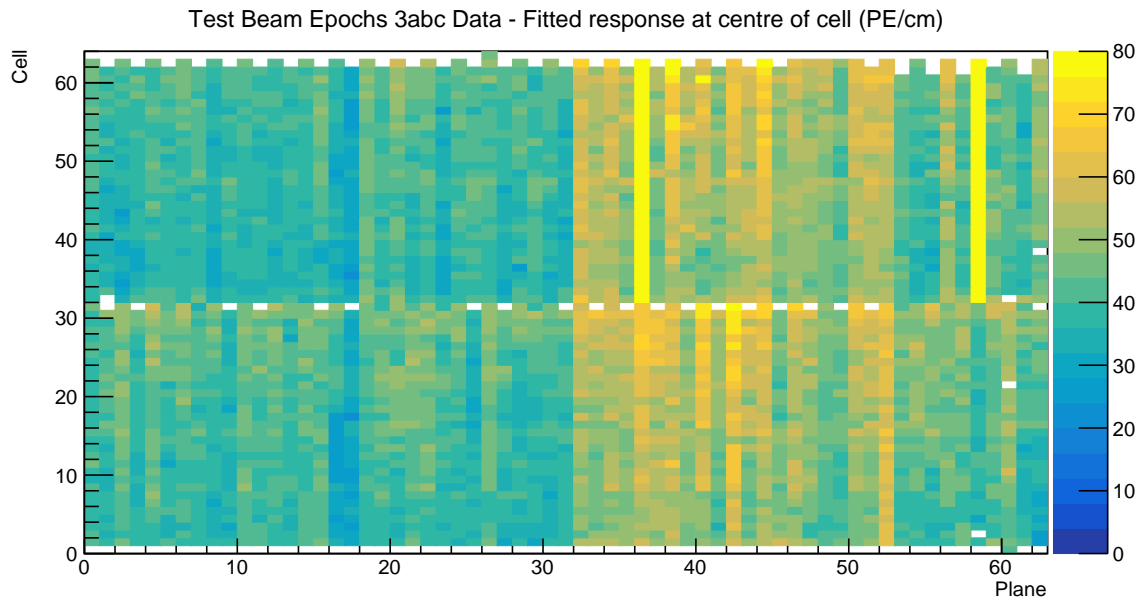


Figure 27: Overview of the relative calibration results for the Teast Beam detector period 3, combined epochs 3a, 3b and 3c data. Each cell represents the result fo the attenuation fit to the energy response in the centre of that cell. The blank cells are uncalibrated.

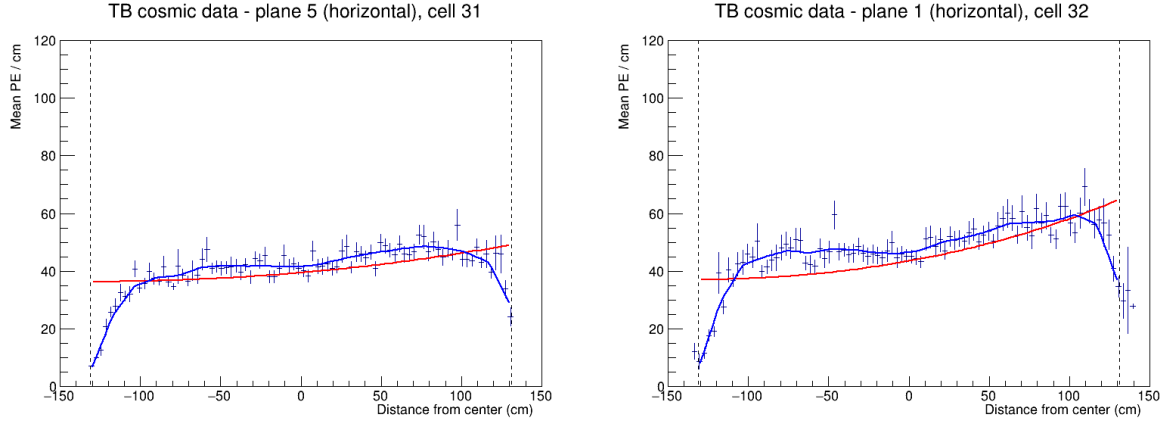


Figure 28: Fit to the energy response in epochs 3 a, b and c. Some underfilled cells that have been refilled in epochs 3b and 3c are now calibrated as shown on the left plot. Cell 32 in plane 1 is the only neighbouring cell to the underfilled cell that didn't manage to get calibrated due to low number of events.

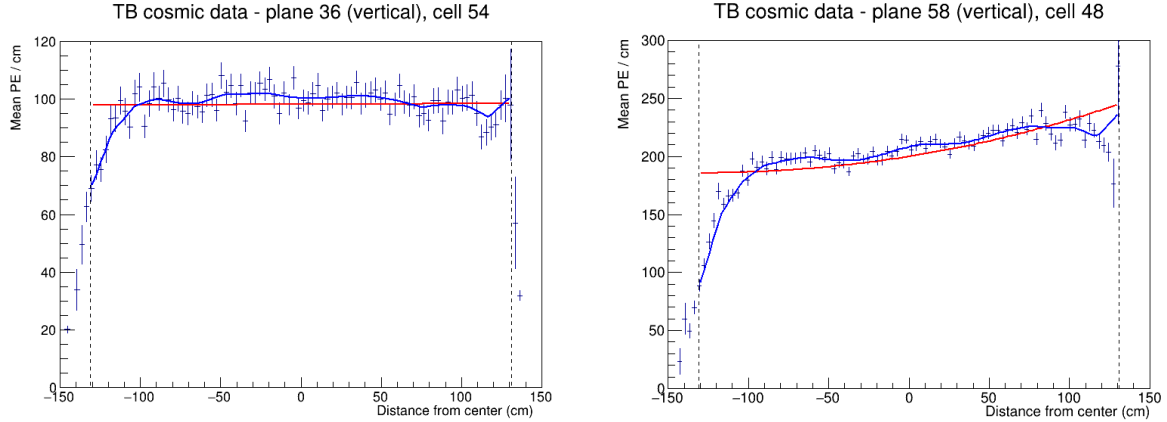


Figure 29: Fit to the energy response in epochs 3 a, b and c. The most obvious faulty FEBs that have a significantly larger energy response than their neighbours.

## 514 4.9 Absolute calibration results

515 Standard absolute calibration cuts: track window, flat-response W, positive pe, pecorr, and  
516 pathlength reco

Sample	NHitsx	MEUx	NHitsy	MEUy	MEU	MEU Err	TrueE/dx	tE/dx Err
epoch 3abc data	2.638e+05	38.49	1.621e+06	39.4	38.94	0.006758	1.772	0.000238
epoch 3de data	1.049e+05	38.63	6.725e+05	39.42	39.02	0.01048	1.772	0.000238
period 2 data	2.322e+05	38.7	1.413e+06	39.4	39.05	0.007252	1.772	0.000238
period 4 data	5.268e+05	38.63	3.316e+06	39.4	39.01	0.004703	1.772	0.000238
simulation	2.829e+05	40.17	1.842e+06	39.93	40.05	0.006418	1.772	0.000238

517

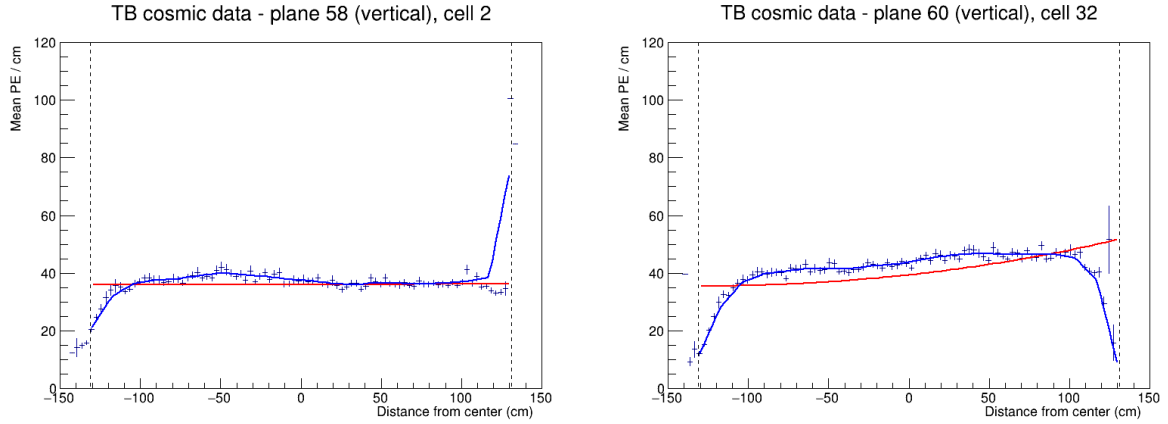


Figure 30: Fit to the energy response in epochs 3 a, b and c. Some cells are not calibrated due to large fluctuations at one edge of the cells.

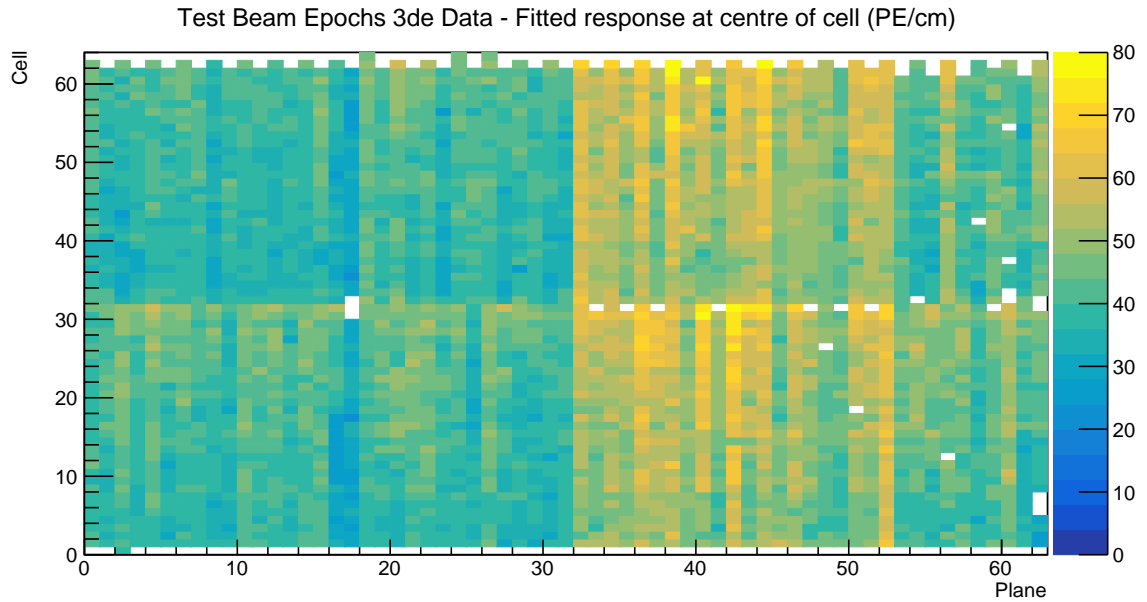


Figure 31: Overview of the relative calibration results for the Teast Beam detector period 3, combined epochs 3d and 3e data. Each cell represents the result fo the attenuation fit to the energy response in the centre of that cell. The blank cells are uncalibrated.

## 518 4.10 Drift in TB data

## 519 4.11 Results

520 Table of final results. Final CSVs are locate in the /nova/ana/testbeam/calibration and  
 521 they have been included in the vXX.XX calibration tag.  
 522 Plots of absolute calibration results

## 523 4.12 Validation

524 Comparisons with older version of calibration and maybe with the FD and ND

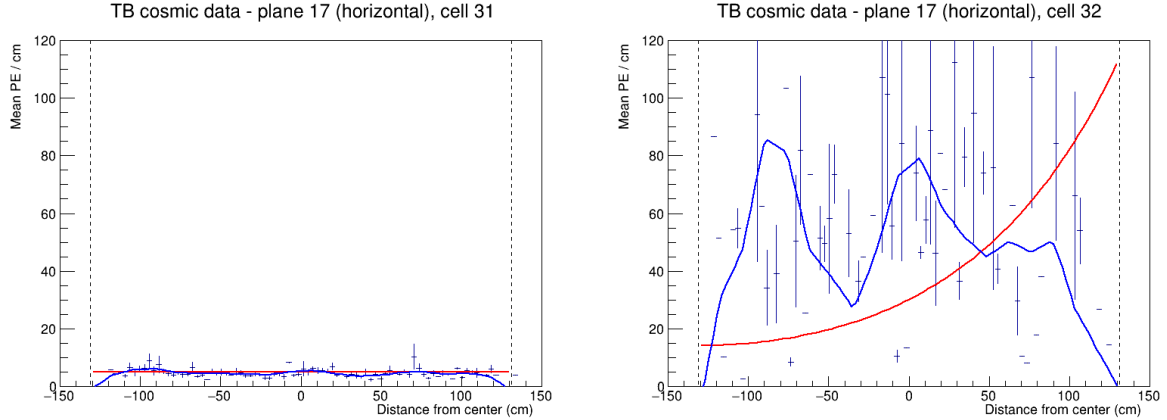


Figure 32: Fit to the energy response in epochs 3 d and e. Possibly dead channel or still underfilled cell.

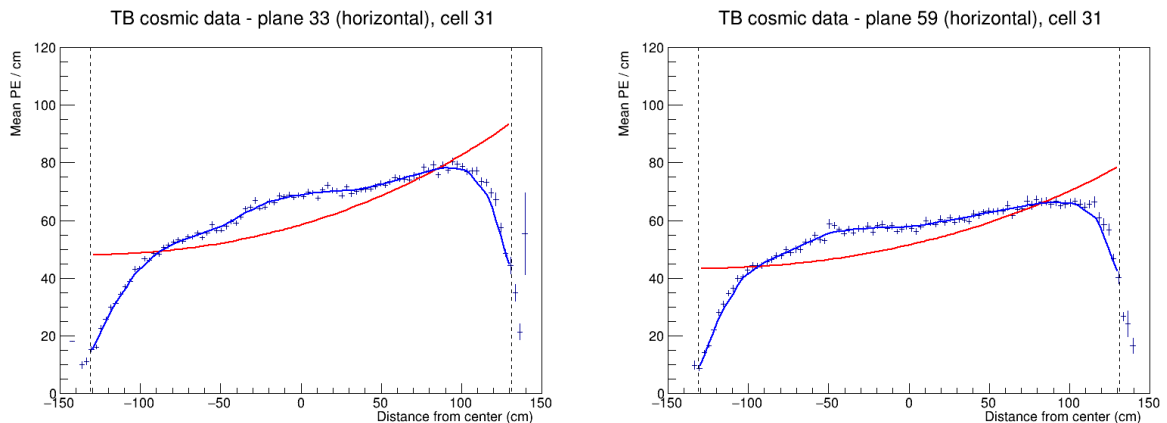


Figure 33: Fit to the energy response in epochs 3 d and e. The scintillator oil used for refilling of the underfilled cells has lower energy response than the oil used for the initial filling. These oils didn't mix properly causing a different energy response in the left and right side of the cell.

## 525 References

- 526 [1] Michael Wallbank. The NOvA Test Beam Program. *PoS*, ICHEP2020:188, 2021. doi:  
527 [10.22323/1.390.0188](https://doi.org/10.22323/1.390.0188).
- 528 [2] Alex Sousa. NOvA Test Beam Status and Plans - Support Documentation. NOVA Doc-  
529 ment 22172-v2, October 2017. NOvA technical note. URL: <https://nova-docdb.fnal.gov/cgi-bin/sso>ShowDocument?docid=22172>.
- 530 [3] Alex Sousa. NOvA Test Beam Plenary @ IU Collaboration Meeting. NOVA Document  
29543, May 2018. NOvA internal document. URL: <https://nova-docdb.fnal.gov/cgi-bin/sso>ShowDocument?docid=29543>.
- 531 [4] Michael Wallbank. Final Test Beam Updates (Geometry and Other!). NOVA Document  
532 58388, April 2023. NOvA internal document. URL: <https://nova-docdb.fnal.gov/cgi-bin/sso>ShowDocument?docid=58388>.

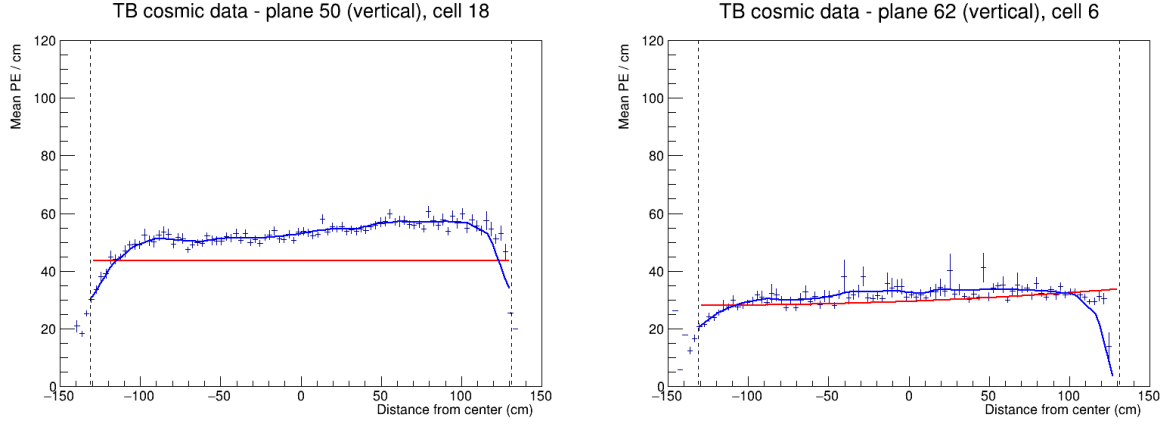


Figure 34: Fit to the energy response in epochs 3 d and e. Some cells have a drop, or a rise of energy response at the edge of the cell. This can be cause by low statistics.

- 537 [5] Michael Wallbank. Understanding, Improving, Validating the Test Beam Geometry.  
538 NOVA Document 57955, February 2023. NOvA internal document. URL: <https://nova-docdb.fnal.gov/cgi-bin/sso>ShowDocument?docid=57955>.
- 540 [6] Robert Kralik. Test beam calibration update. NOVA Document 57516-v2, January  
541 2023. NOvA internal document. URL: <https://nova-docdb.fnal.gov/cgi-bin/sso>ShowDocument?docid=57516>.
- 543 [7] Alex Sousa. Test Beam Plenary Update - Jun. 6, 2019. NOVA Document 38349, June  
544 2019. NOvA internal document. URL: <https://nova-docdb.fnal.gov/cgi-bin/sso>ShowDocument?docid=38349>.
- 546 [8] Alex Sousa. Test Beam Plenary Update - FNAL September 2018. NOVA Document  
547 33012, September 2018. NOvA internal document. URL: <https://nova-docdb.fnal.gov/cgi-bin/sso>ShowDocument?docid=33012>.
- 549 [9] Alex Sousa. Filling System and Scintillator Status. NOVA Document 34067, November  
550 2018. NOvA internal document. URL: <https://nova-docdb.fnal.gov/cgi-bin/sso>ShowDocument?docid=34067>.
- 552 [10] Junting Huang, Will Flanagan, and Beatriz Tapia Oregui. Test Beam: Light Yield of  
553 the Liquid Scintillator Drained from the NDOS Detector. NOVA Document 38740, July  
554 2019. NOvA internal document. URL: <https://nova-docdb.fnal.gov/cgi-bin/sso>ShowDocument?docid=38740>.
- 556 [11] Dung Phan. Test Beam: Tintometer Measurement of Texas A&M oil. NOVA Document  
557 39088, July 2019. NOvA internal document. URL: <https://nova-docdb.fnal.gov/cgi-bin/sso>ShowDocument?docid=39088>.
- 559 [12] Alex Sousa. Test Beam Scintillator Fill Plan. NOVA Document 34196, November  
560 2018. NOvA internal document. URL: <https://nova-docdb.fnal.gov/cgi-bin/sso>ShowDocument?docid=34196>.

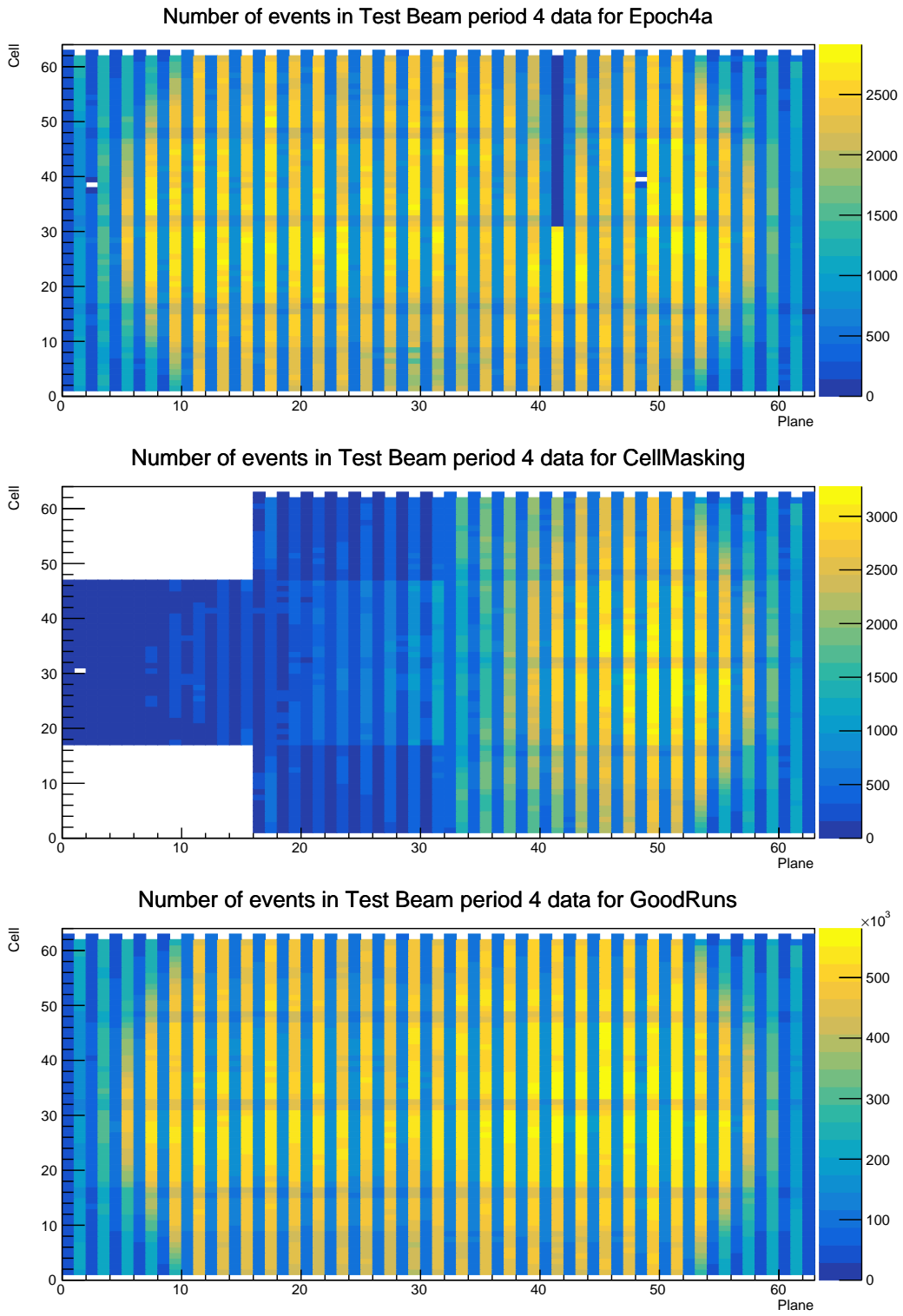


Figure 35: Distribution of events in the Test Beam period 4 data calibration sample. The top plot shows the first three commissioning runs, the middle plot the status of the detector during the Cell Masking studies and the bottom plot shows the rest.

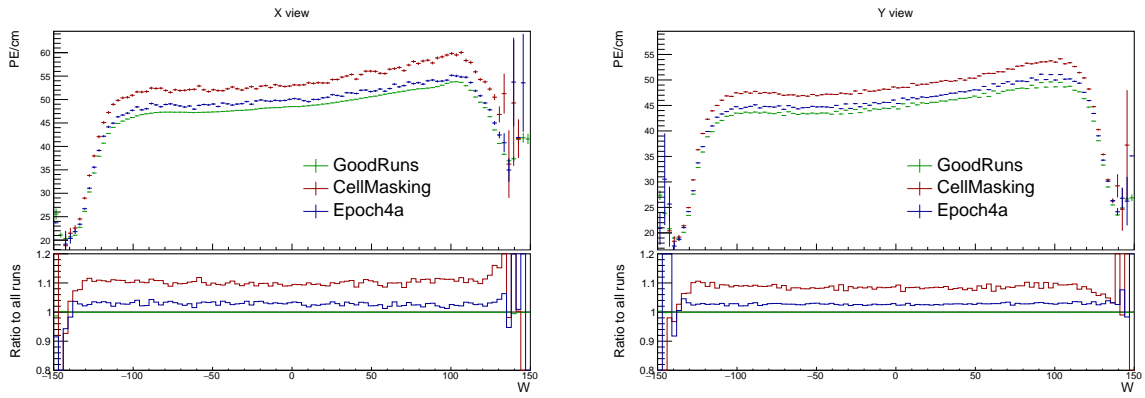


Figure 36: Uncorrected average energy response as a function of the position within a cell ( $w$ ) for epochs in period 4.

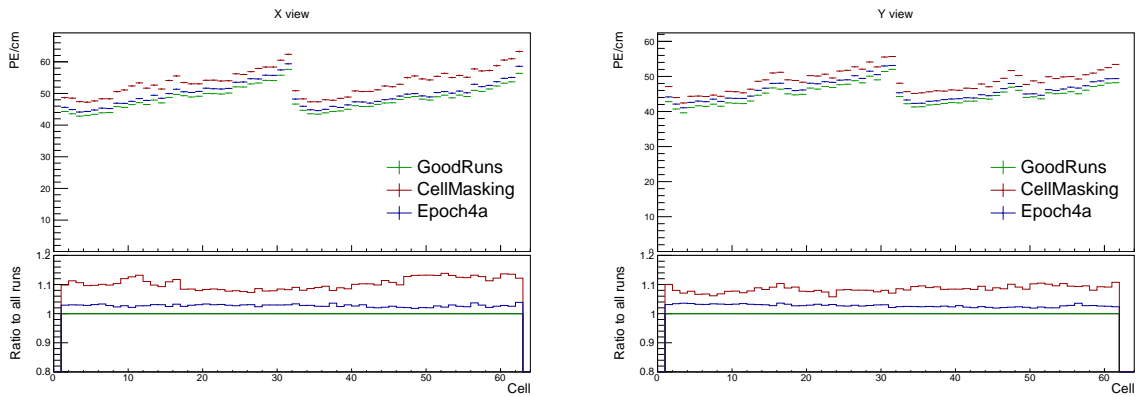


Figure 37: Uncorrected average energy response as a function of cells for epochs in period 4.

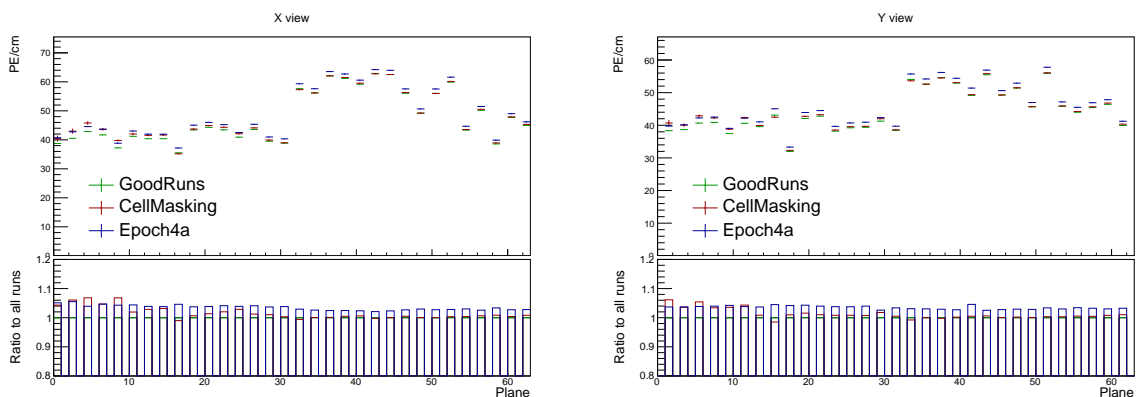


Figure 38: Uncorrected average energy response as a function of planes for epochs in period 4.

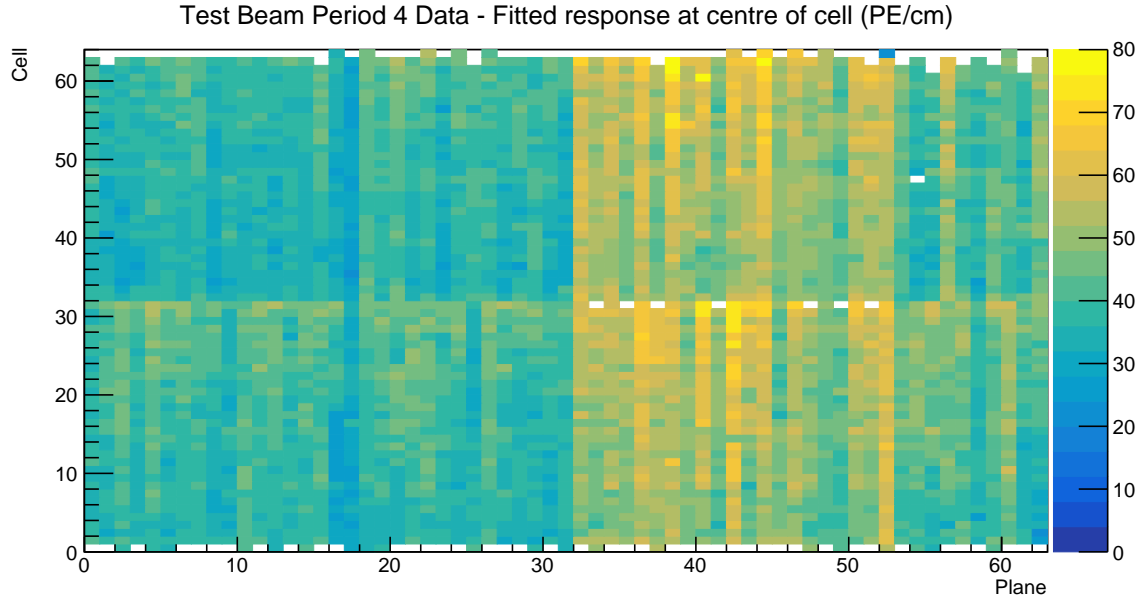


Figure 39: Overview of the relative calibration results for the Teast Beam detector period 4 data. Each cell represents the result fo the attenuation fit to the energy response in the centre of that cell. The blank cells are uncalibrated.

- 562 [13] Karol Lang. NOvA Test Beam: To mix, or not to mix, that is the question. NOVA Document  
563 34046-v2, November 2018. NOvA technical note. URL: <https://nova-docdb.fnal.gov/cgi-bin/sso>ShowDocument?docid=34046>.
- 565 [14] Alex Sousa. 2nd Block Filling Status - Nov. 18, 2019. NOVA Document 41961, November  
566 2019. NOvA internal document. URL: <https://nova-docdb.fnal.gov/cgi-bin/sso>ShowDocument?docid=41961>.
- 568 [15] Teresa Megan Lackey. *Proton Scattering in NOvA Test Beam*. PhD thesis, Indiana U.,  
569 July 2022.
- 570 [16] David Northacker, Alex Sousa, and Yagmur Torun. Test Beam - Overfilling Horizontal  
571 Planes. NOVA Document 49439, March 2021. NOvA internal document. URL: <https://nova-docdb.fnal.gov/cgi-bin/sso>ShowDocument?docid=49439>.
- 573 [17] Keith Matera et al. Calibration Technotes. NOVA Document 13579, January  
574 2017. NOvA technical note. URL: <https://nova-docdb.fnal.gov/cgi-bin/sso>ShowDocument?docid=13579>.
- 576 [18] Christopher J. Backhouse. Cell-by-cell attenuation calibration of the NOvA detectors.  
577 NOVA Document 7410, December 2014. NOvA technical note. URL: <https://nova-docdb.fnal.gov/cgi-bin/sso>ShowDocument?docid=7410>.
- 579 [19] Evan David Niner. *Observation of Electron Neutrino Appearance in the NuMI Beam with  
580 the NOvA Experiment*. PhD thesis, Indiana U., 2015. doi:10.2172/1221353.

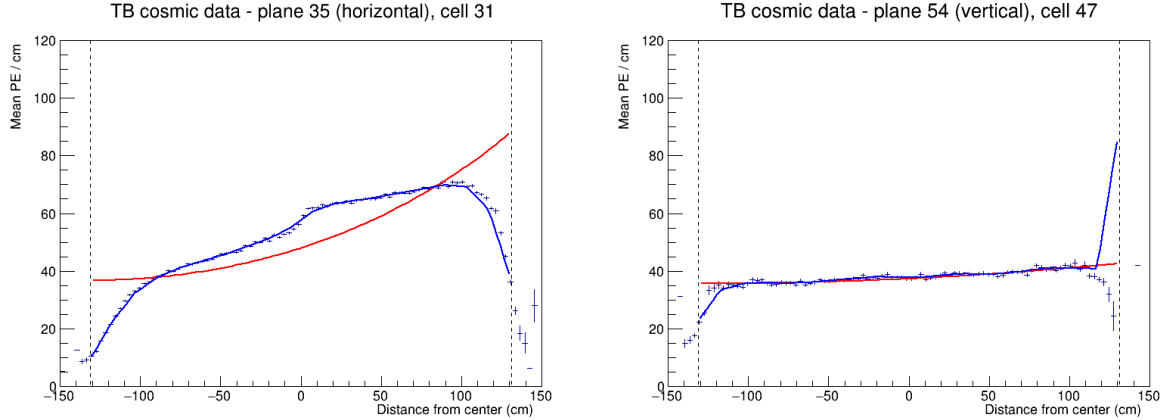


Figure 40: Fit to the energy response in period 4. Previously underfilled cells refilled with a scintillator of a different quality causing an unusual distribution of energy deposition (left). Unusually high energy response at the edge of the cell 47 (right).

- 581 [20] Christopher J. Backhouse. Timing bias introduced by incorrect interpretation of the  
582 nanoslice. NOVA Document 13518, June 2015. NOvA technical note. URL: <https://nova-docdb.fnal.gov/cgi-bin/sso>ShowDocument?docid=13518>.
- 584 [21] Luke Vinton. Calorimetric Energy Scale Calibration of the NOvA Detectors. NOVA Doc-  
585 ument 13579, document FA\_Calorimetric\_energy\_scale.pdf, July 2015. NOvA technical  
586 note. URL: <https://nova-docdb.fnal.gov/cgi-bin/sso>ShowDocument?docid=13579>.
- 588 [22] Keith Matera. Keith's Swell Guide: The Calibration Meta. NOVA Document 13579, doc-  
589 ument Calibration\_Meta\_READFIRST.pdf, January 2017. NOvA technical note. URL:  
590 <https://nova-docdb.fnal.gov/cgi-bin/sso>ShowDocument?docid=13579>.
- 591 [23] Christopher Backhouse, Alexender Radovic, and Prabhjot Singh. The Attenuation and  
592 Threshold Calibration of the NOvA detectors. NOVA Document 13579, document  
593 SA\_Attenuation\_and\_Threshold.pdf, May 2016. NOvA technical note. URL: <https://nova-docdb.fnal.gov/cgi-bin/sso>ShowDocument?docid=13579>.
- 595 [24] Ryan J. Nichol. Fibre brightness from cosmic muon data. NOVA Document 34909, De-  
596 cember 2018. NOvA technical note. URL: [https://nova-docdb.fnal.gov/cgi-bin/](https://nova-docdb.fnal.gov/cgi-bin/sso/)  
597 [ShowDocument?docid=34909](https://nova-docdb.fnal.gov/cgi-bin/sso>ShowDocument?docid=34909).
- 598 [25] Anna Maureen Hall. TB P2 Calib. Summary. NOVA Document 49674, March 2021.  
599 NOvA internal document. URL: [https://nova-docdb.fnal.gov/cgi-bin/](https://nova-docdb.fnal.gov/cgi-bin/sso/)  
600 [ShowDocument?docid=49674](https://nova-docdb.fnal.gov/cgi-bin/sso>ShowDocument?docid=49674).
- 601 [26] Matthew Strait. Update on light level tuning. NOVA Document 43249, February  
602 2020. NOvA internal document. URL: [https://nova-docdb.fnal.gov/cgi-bin/](https://nova-docdb.fnal.gov/cgi-bin/sso/)  
603 [ShowDocument?docid=43249](https://nova-docdb.fnal.gov/cgi-bin/sso>ShowDocument?docid=43249).

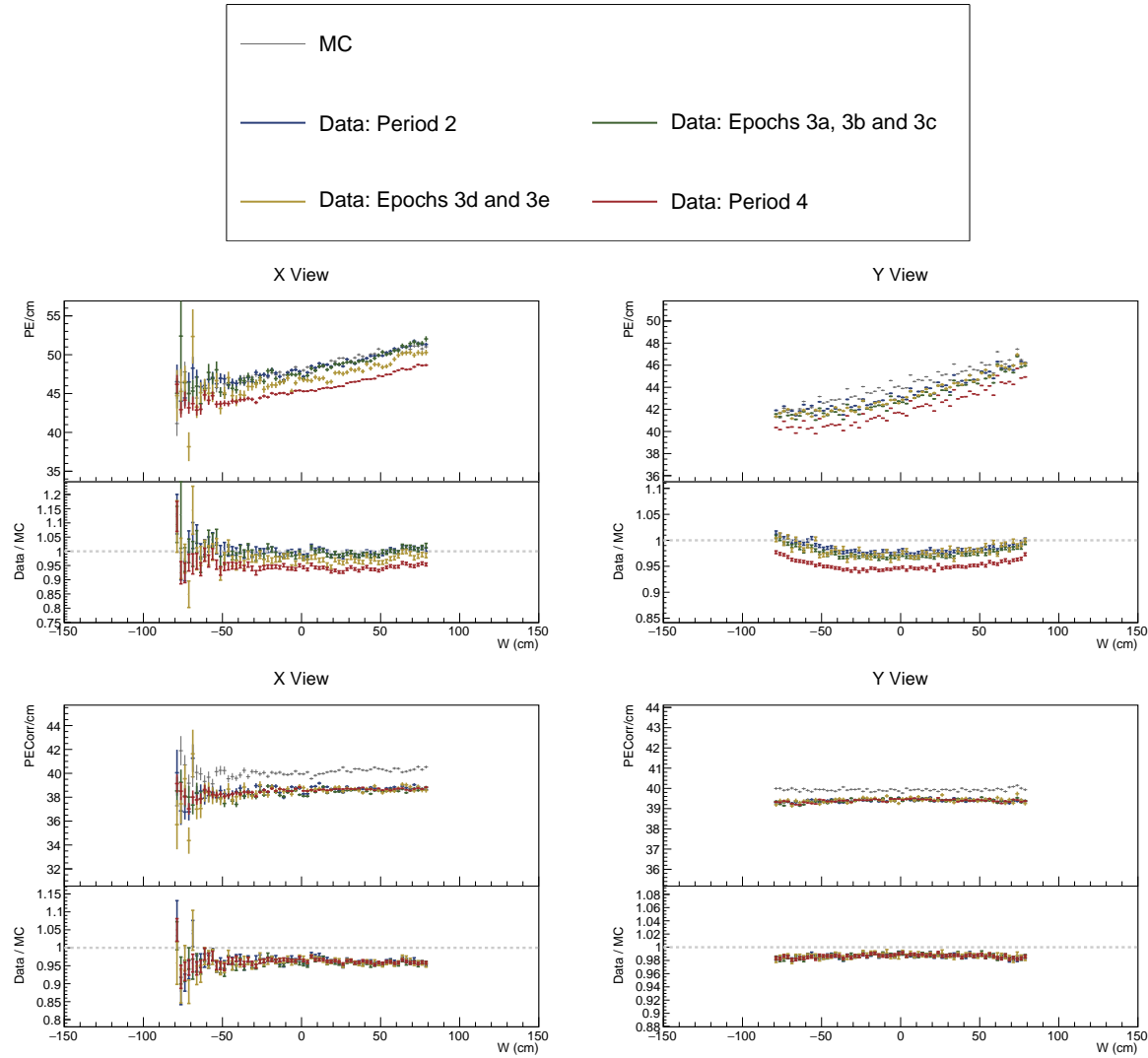


Figure 41: ...

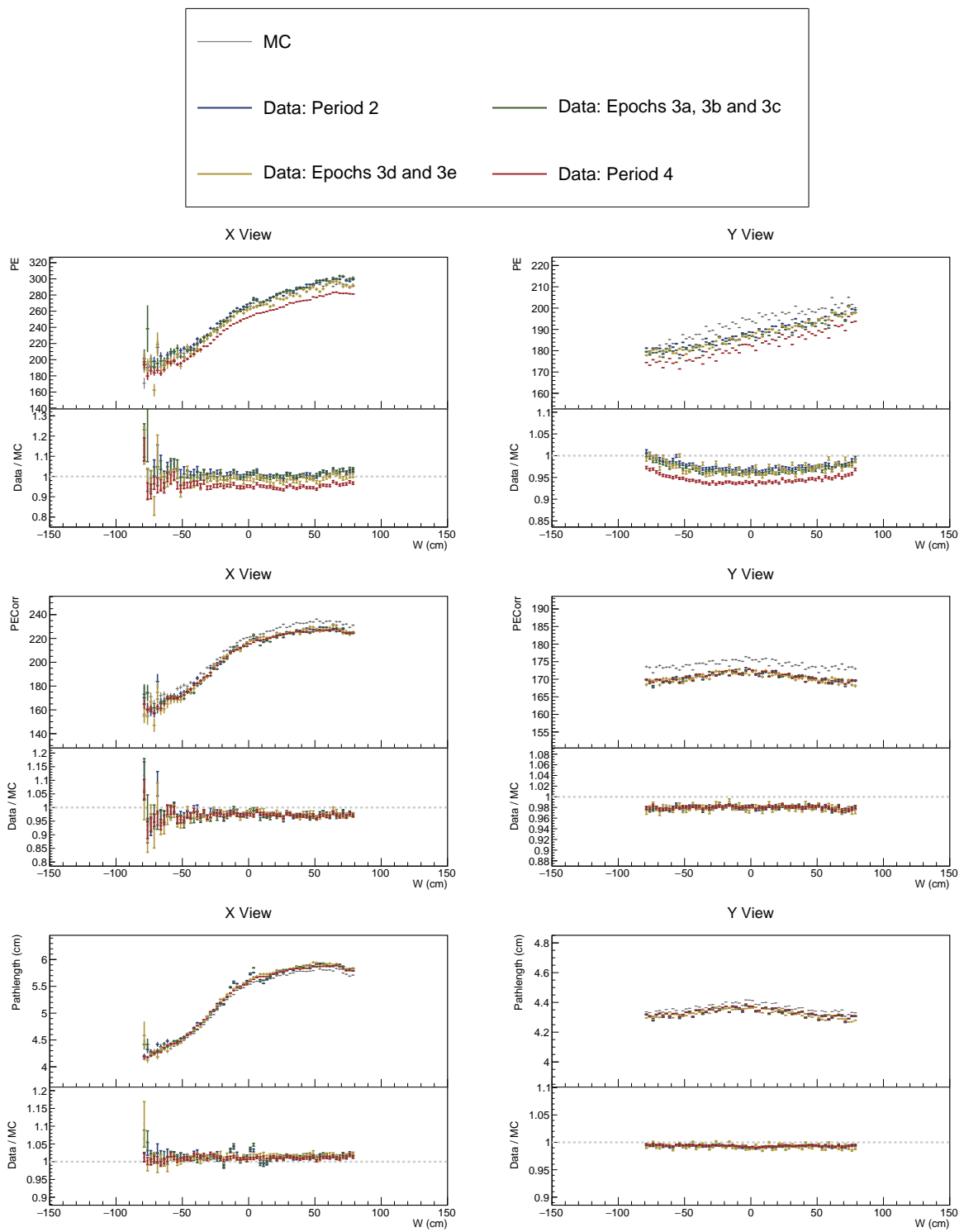


Figure 42: ...

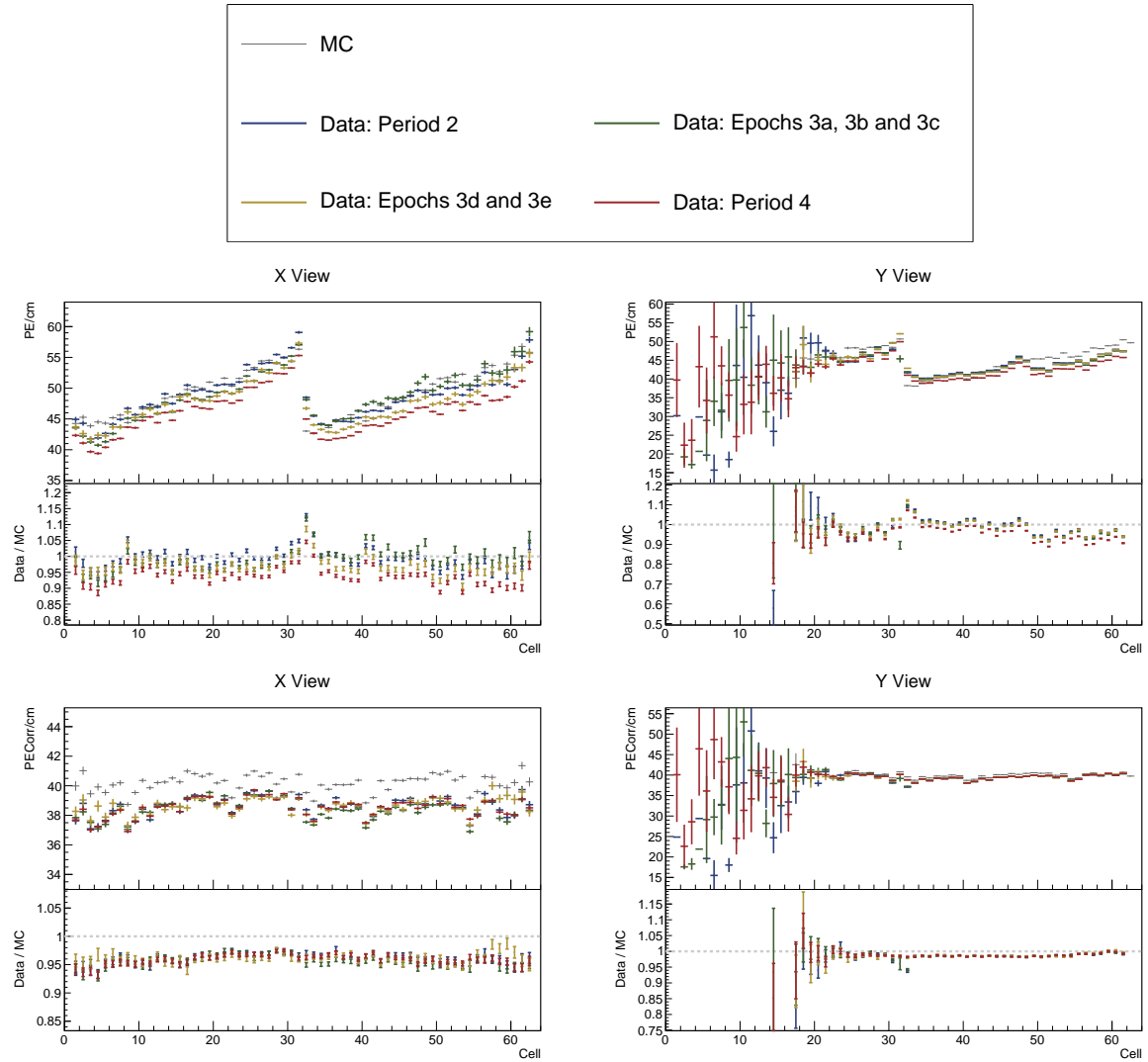


Figure 43: ...

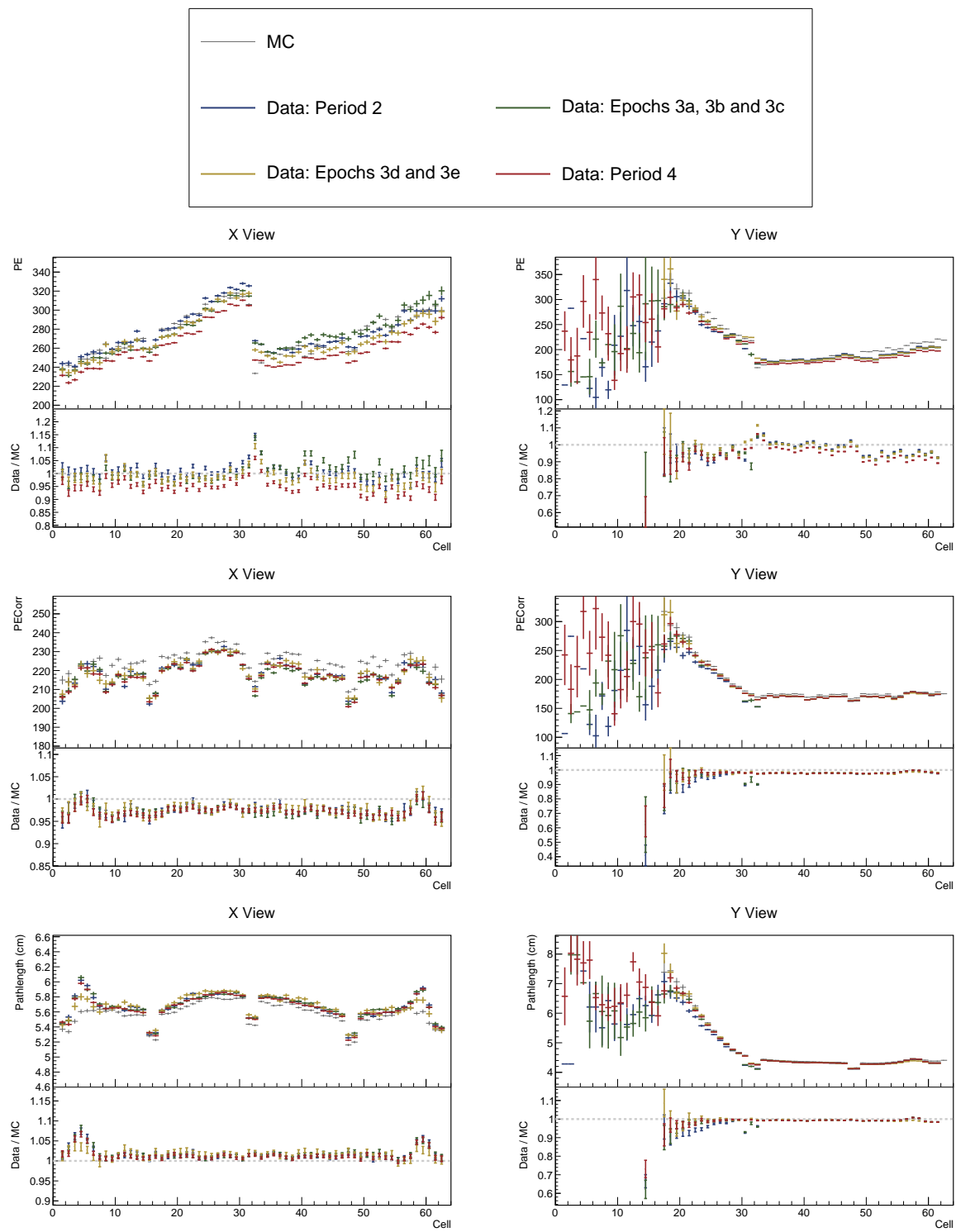


Figure 44: ...

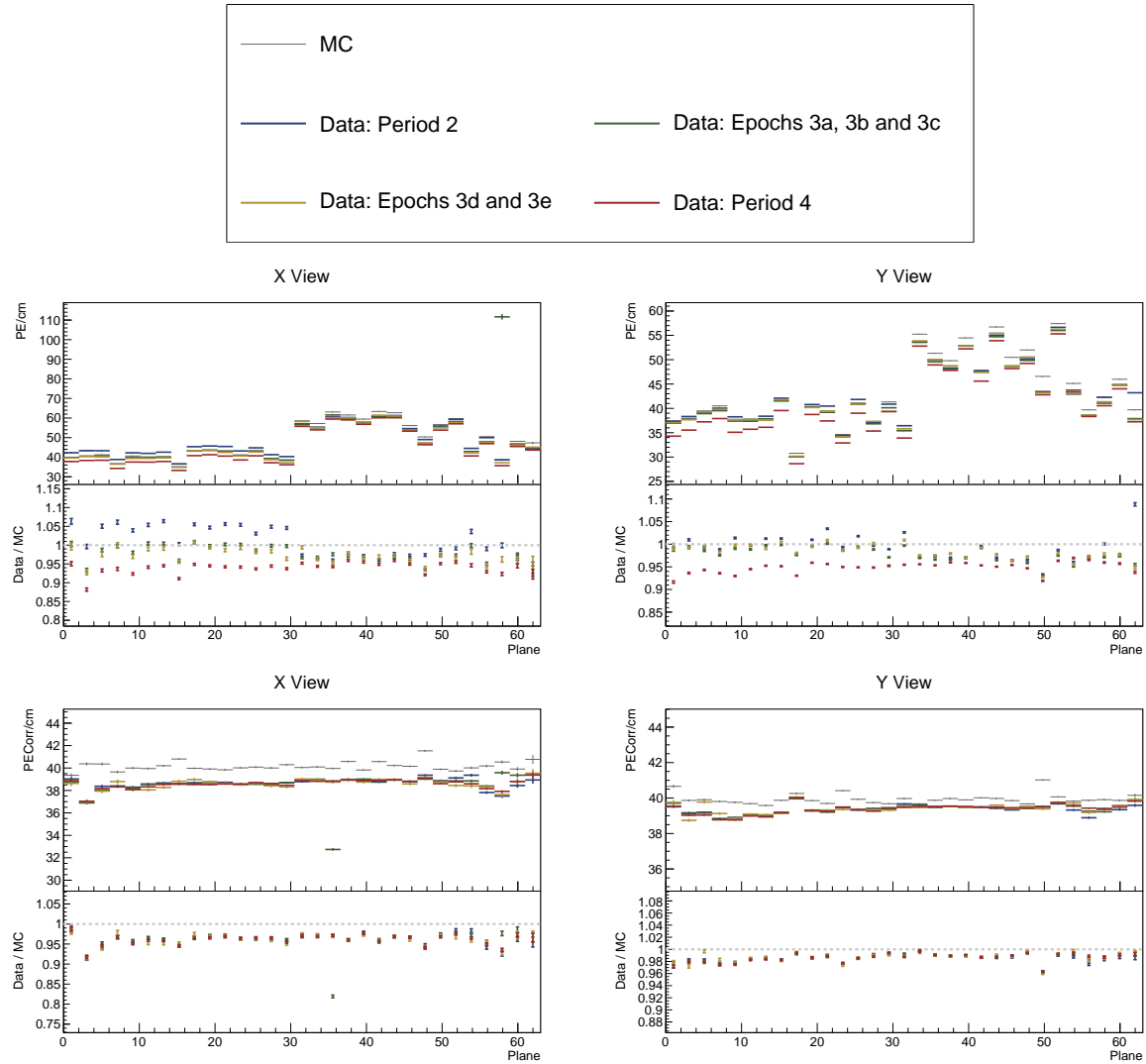


Figure 45: ...

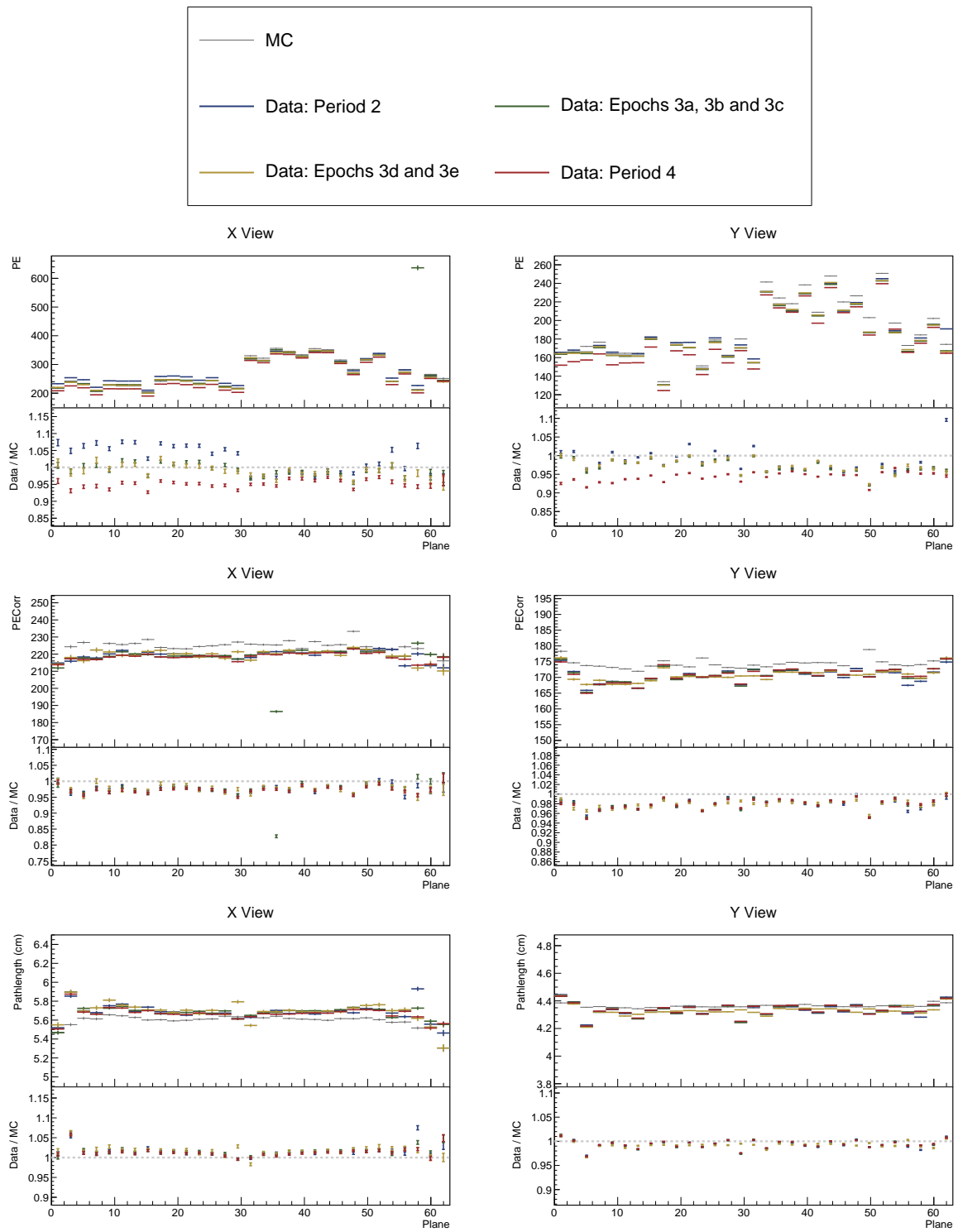


Figure 46: ...

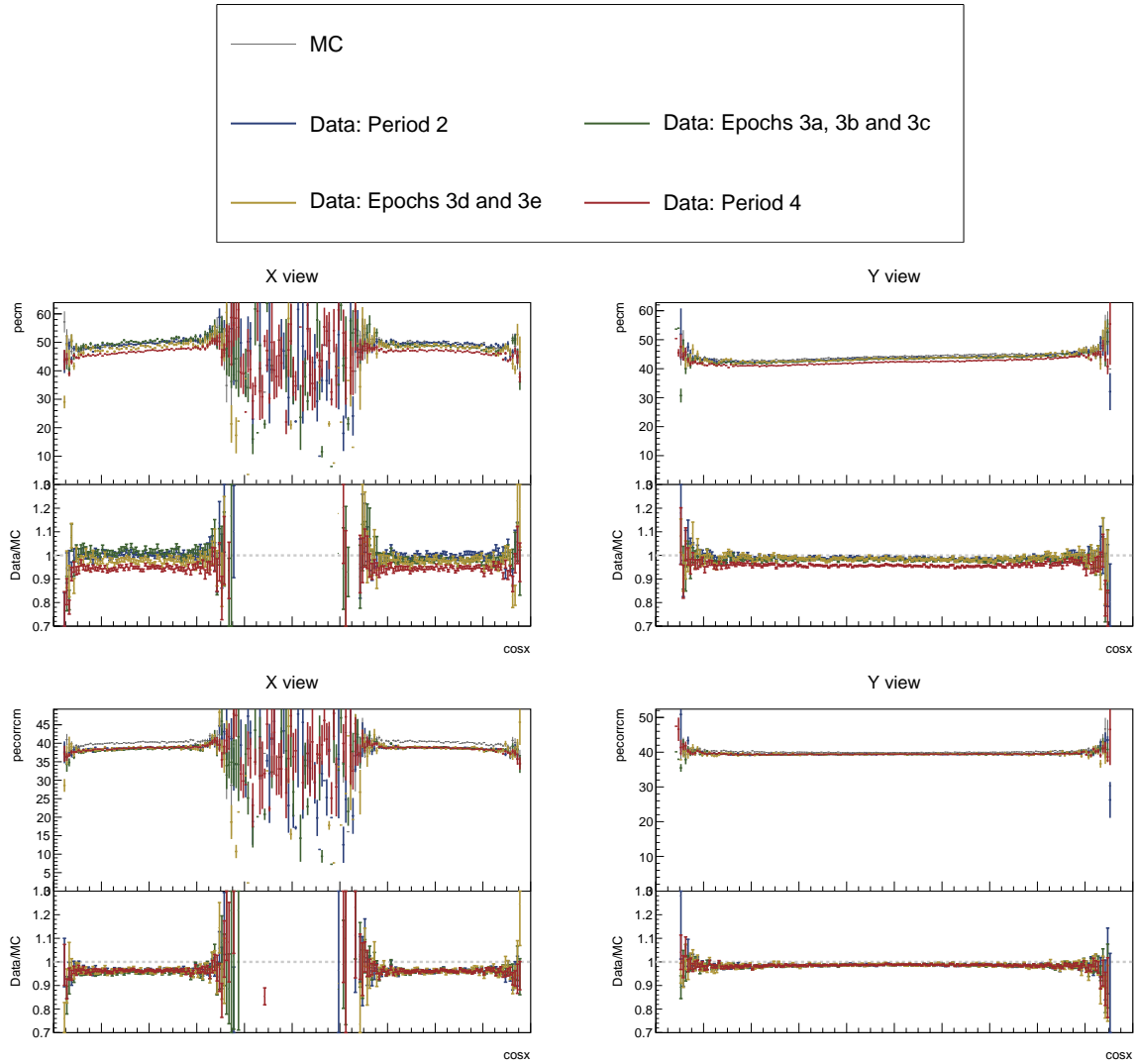


Figure 47: ...

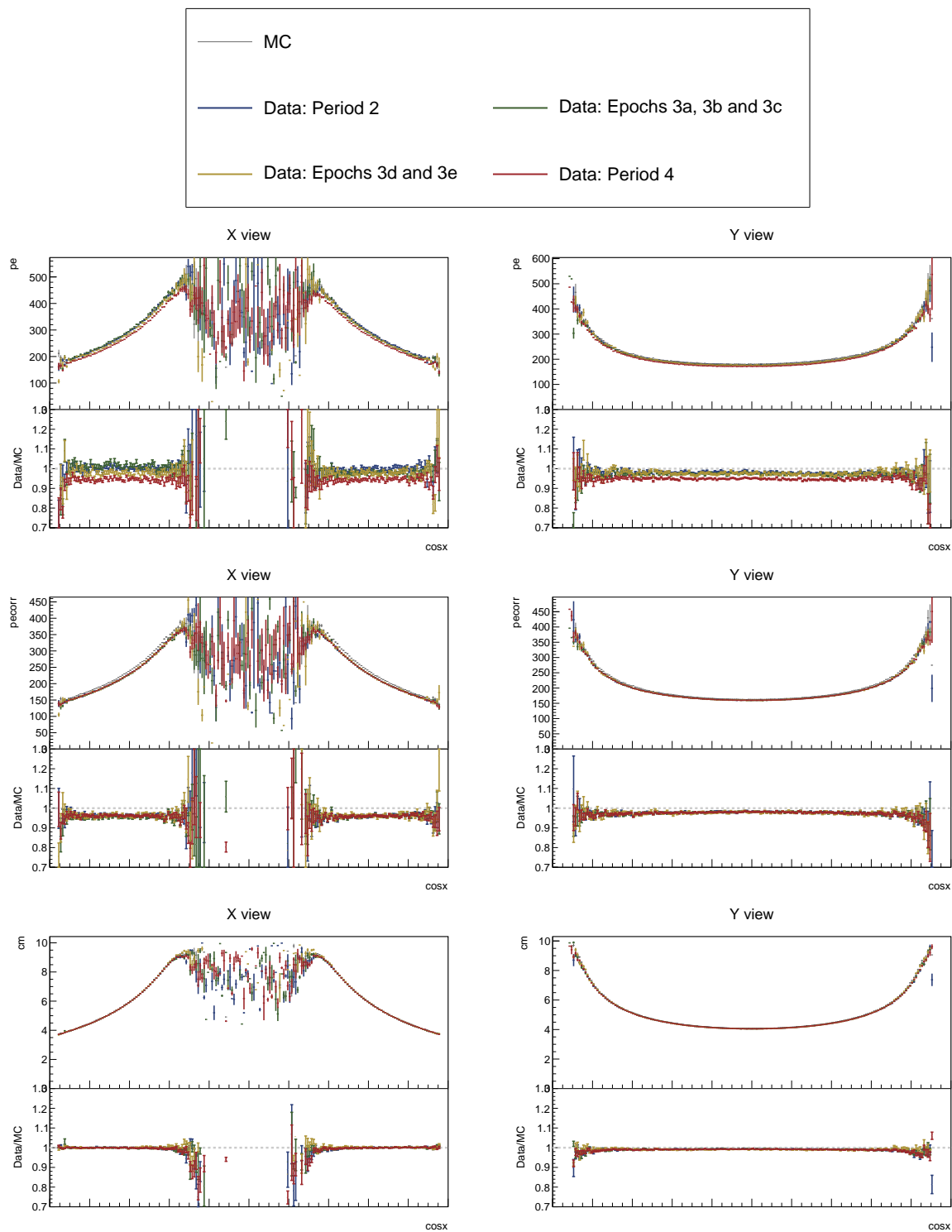


Figure 48: ...

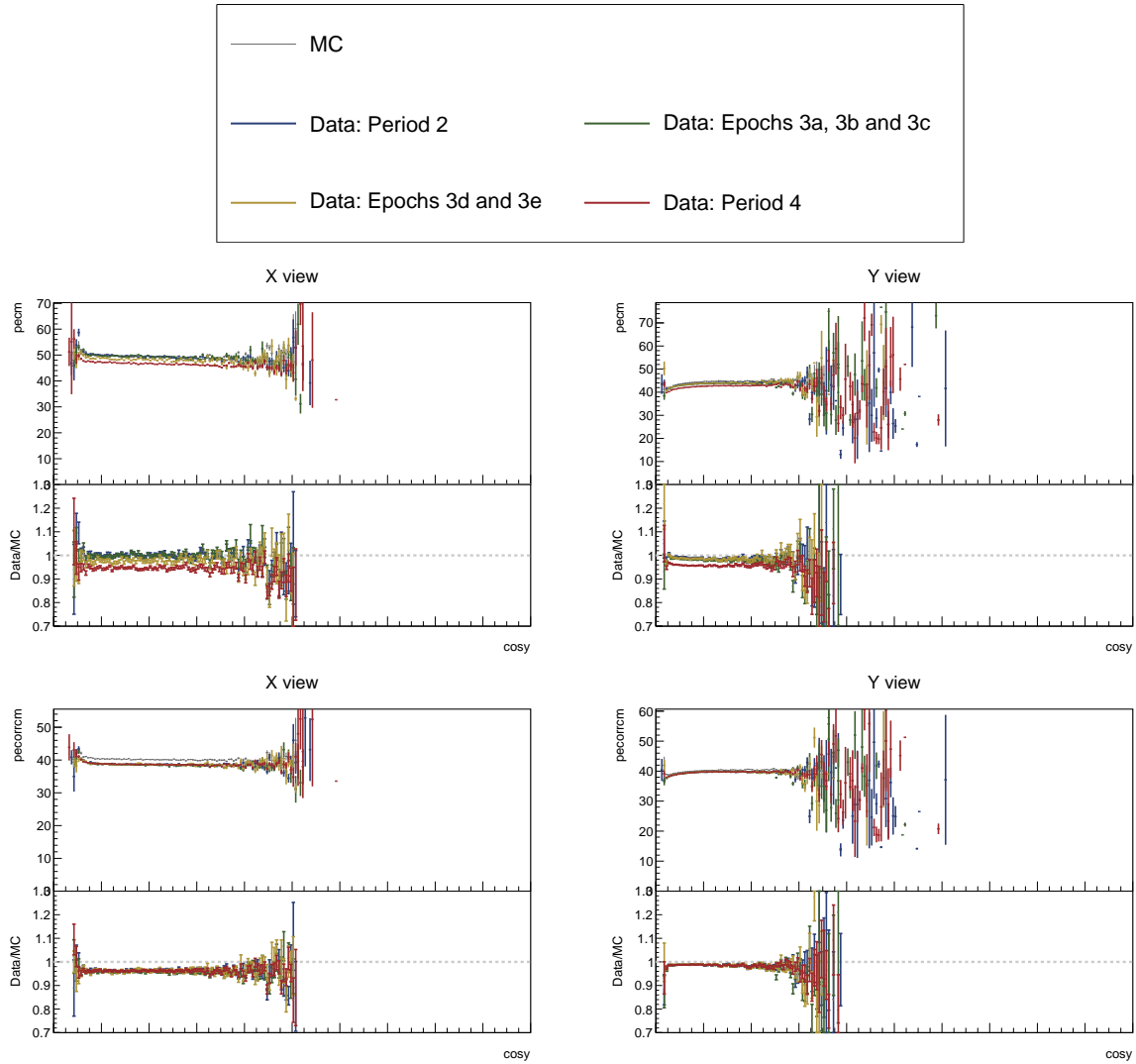


Figure 49: ...

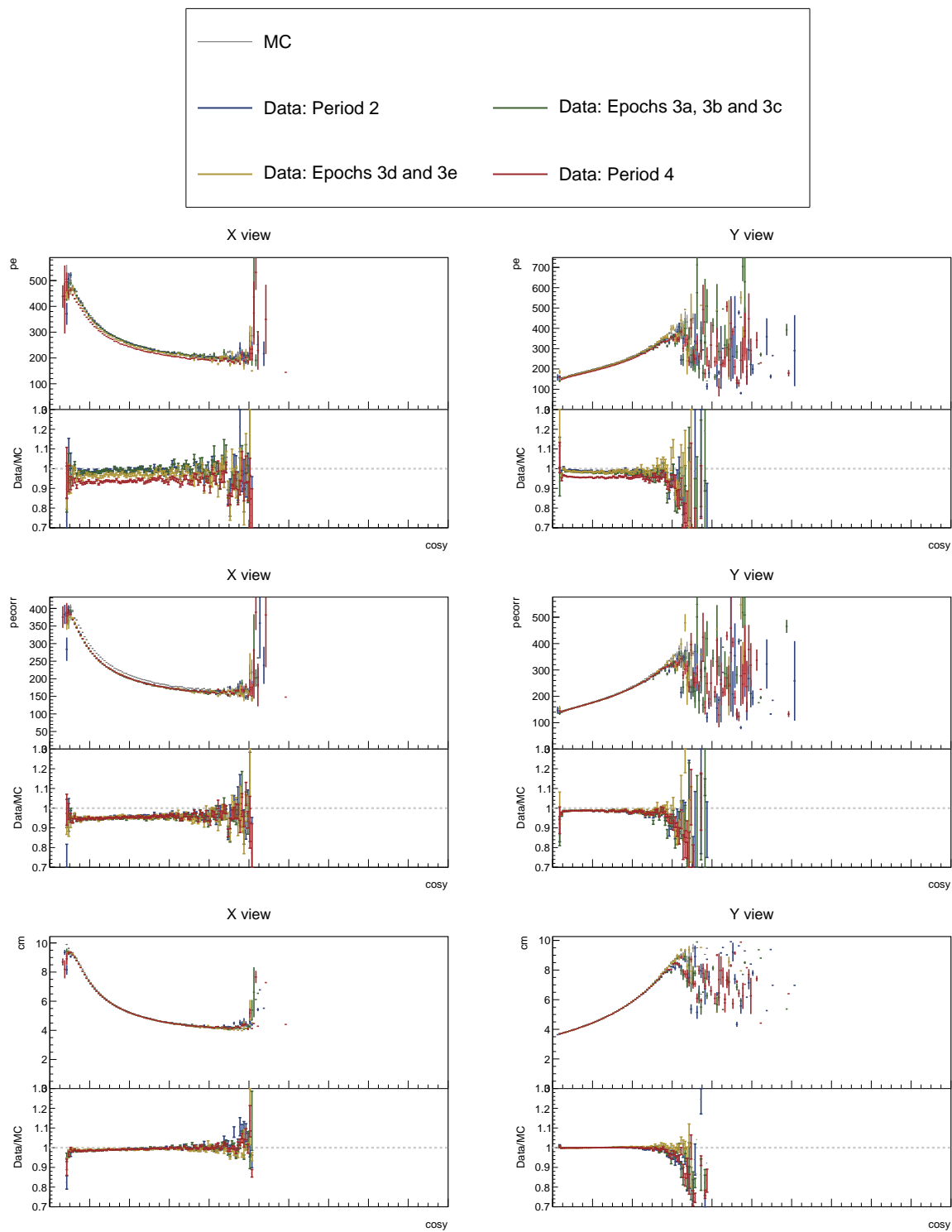


Figure 50: ...

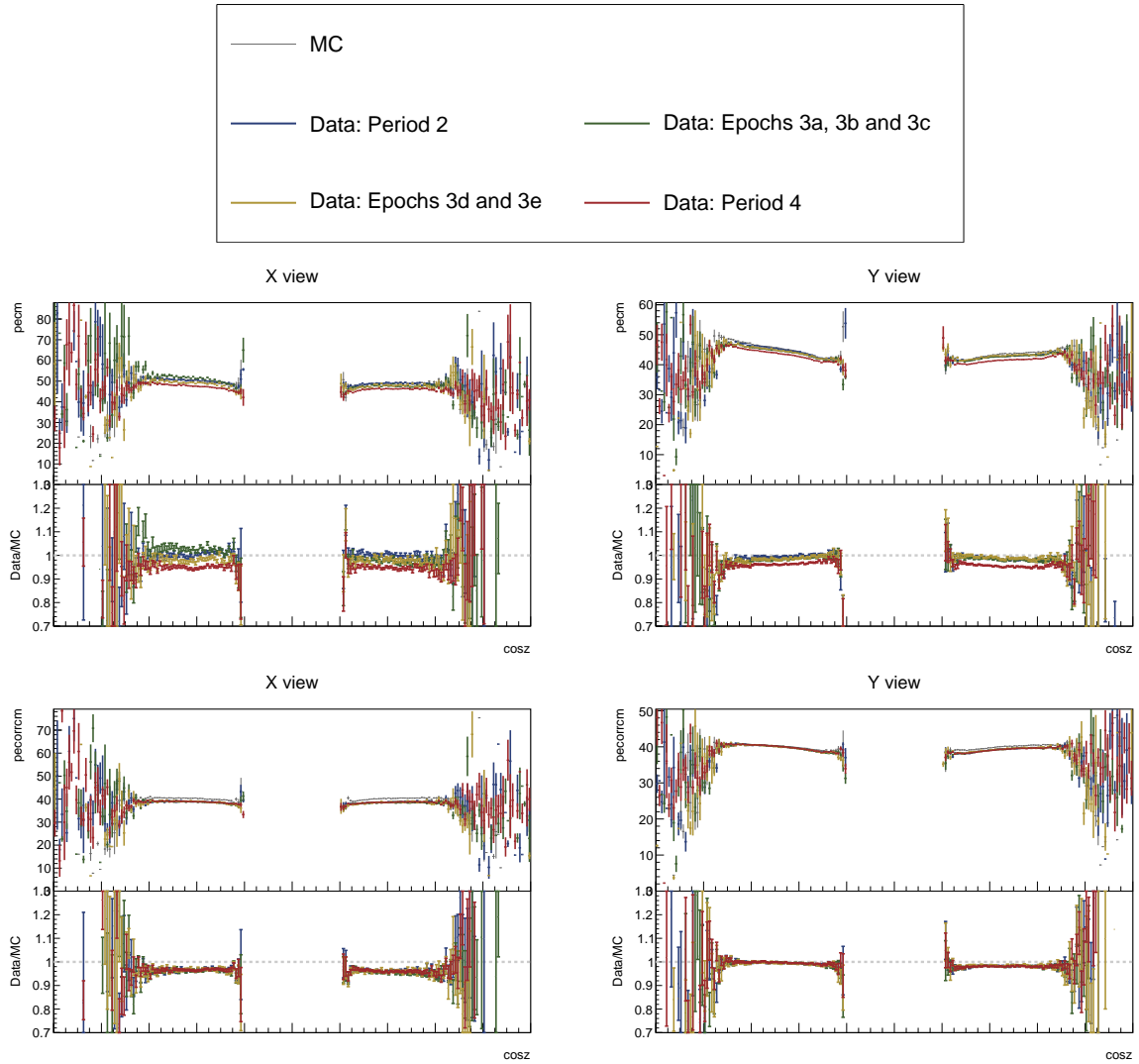


Figure 51: ...

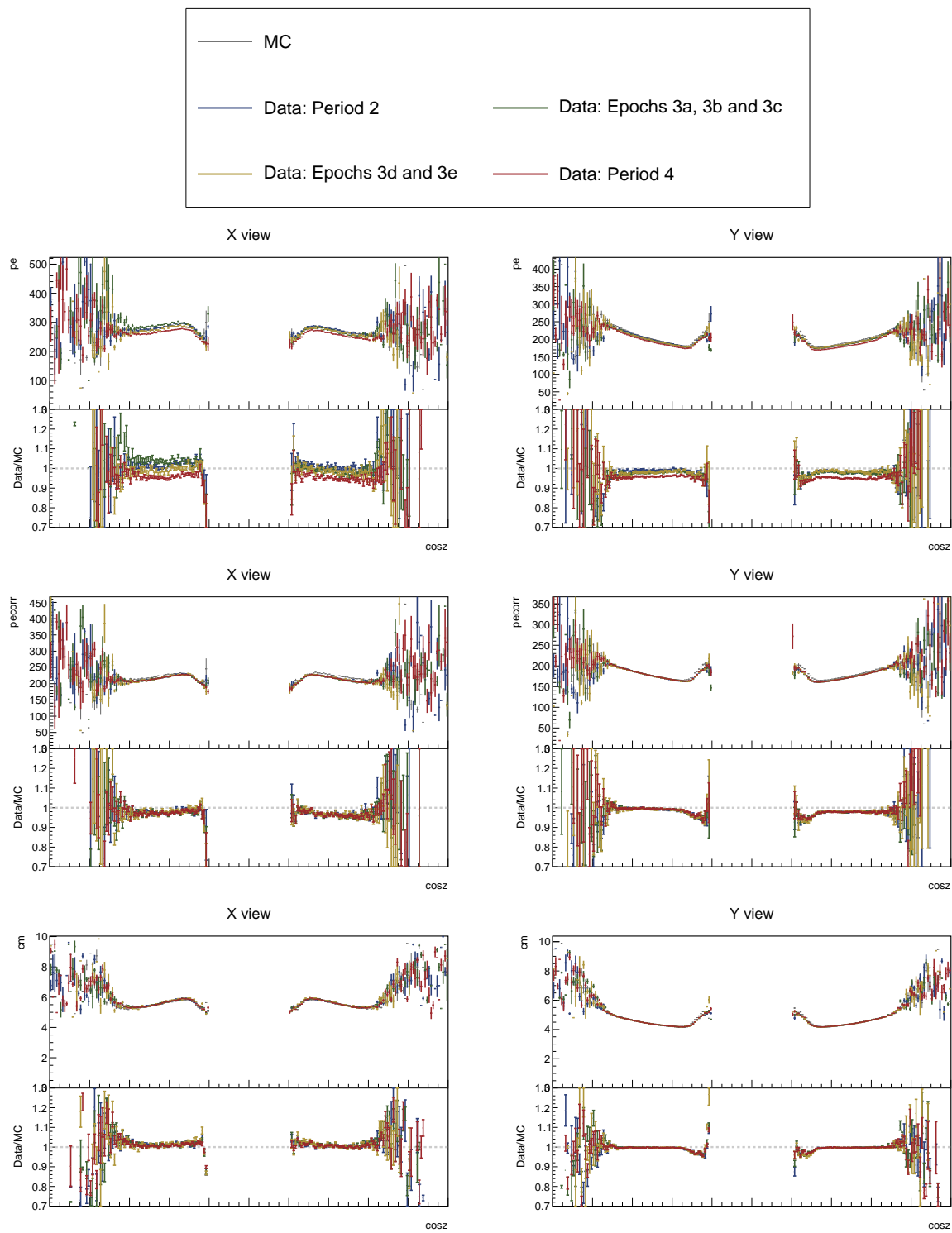


Figure 52: ...

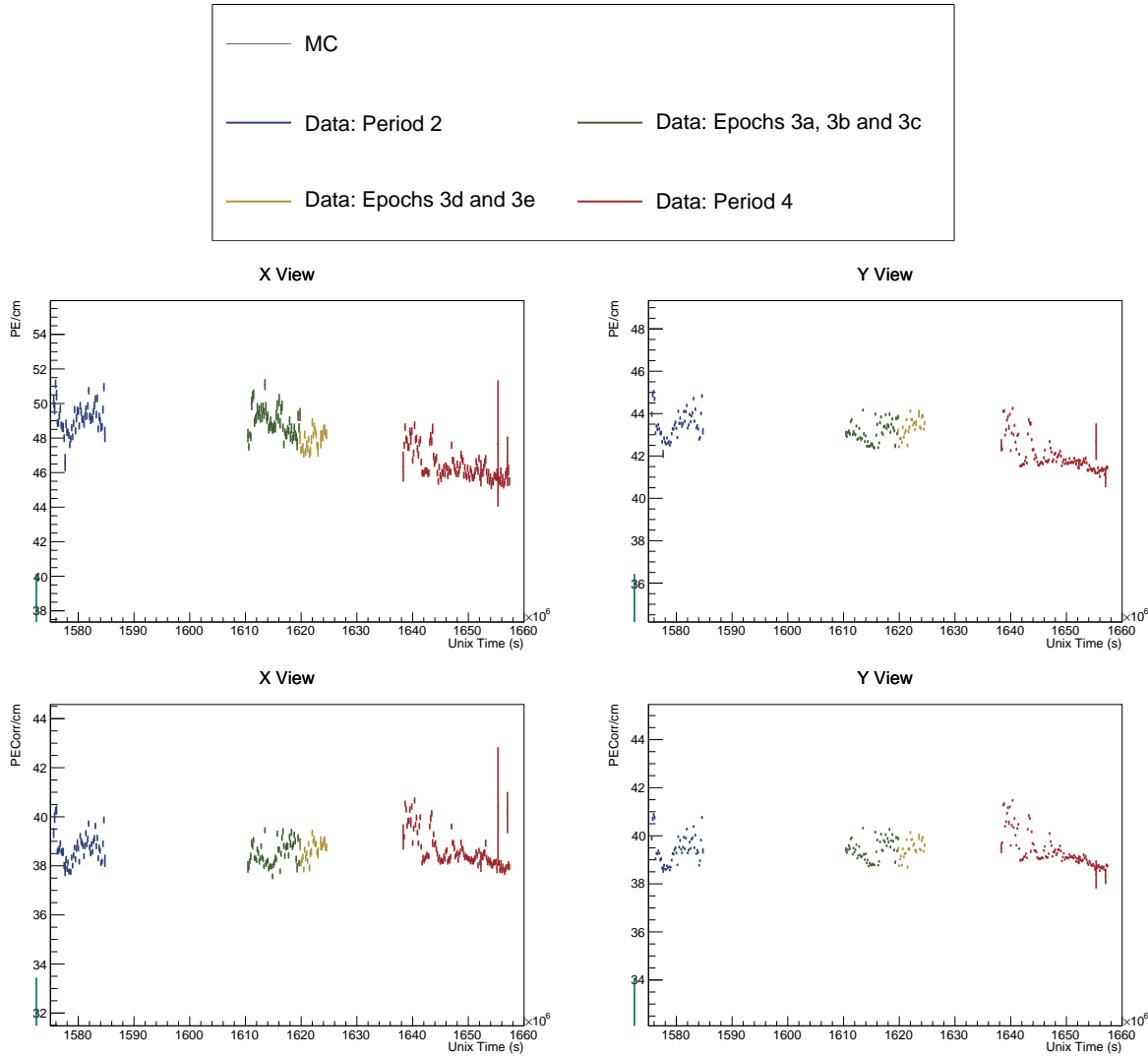


Figure 53: ...

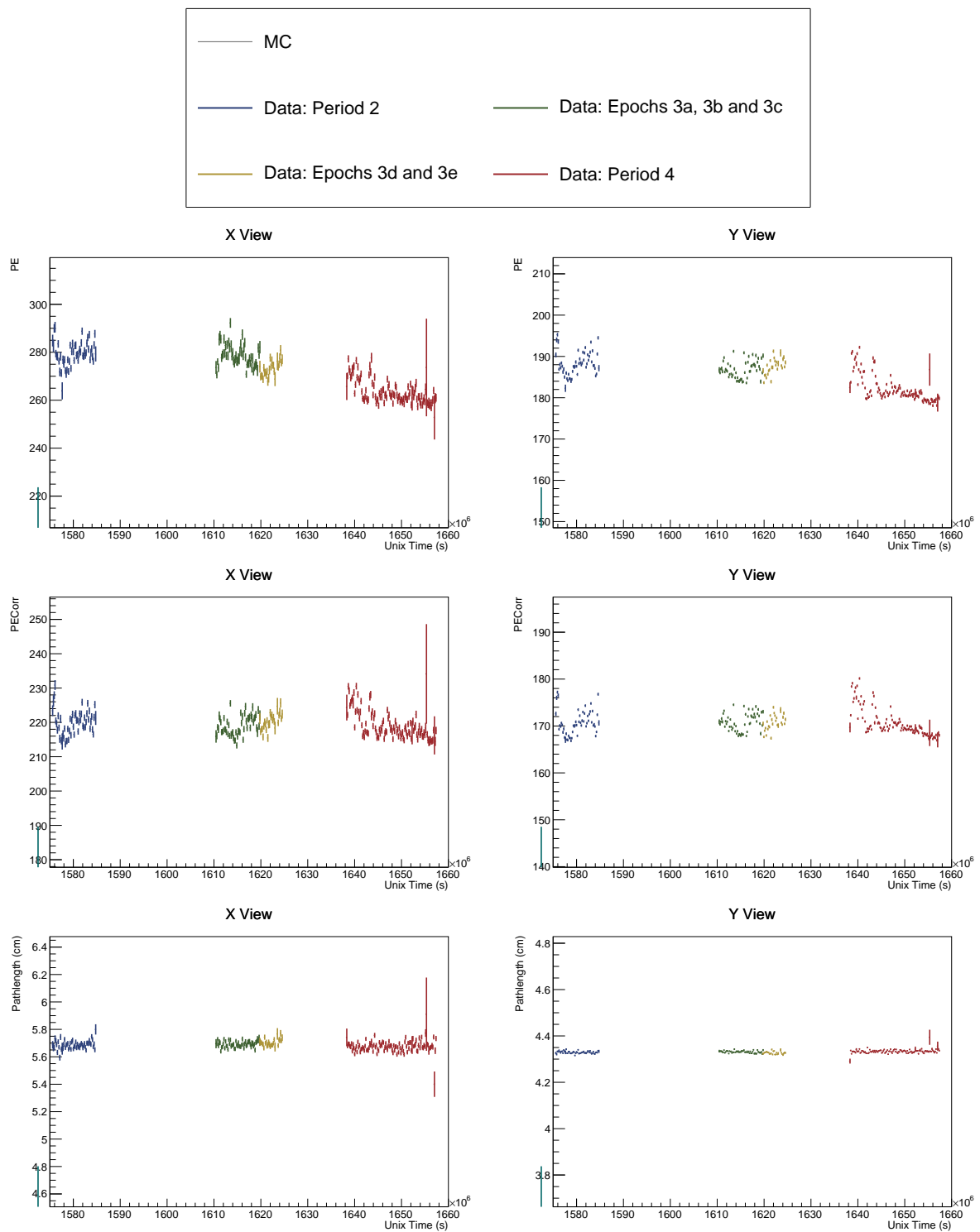


Figure 54: ...